THE JOURNAL OF BIOLOGICAL CHEMISTRY VOL. 286, NO. 45, pp. 38948–38959, November 11, 2011

Understanding the Kinetic Roles of the Inducer Heparin and of Rod-like Protofibrils during Amyloid Fibril Formation by Tau Protein*[S]

Received for publication, June 14, 2011, and in revised form, September 13, 2011 Published, JBC Papers in Press, September 20, 2011, DOI 10.1074/jbc.M111.271874

Gayathri Ramachandran[1] **and Jayant B. Udgaonkar**[2]

From the National Centre for Biological Sciences, Tata Institute of Fundamental Research, Bangalore 560065, India

Background: The kinetic role of heparin and of intermediates populated during Tau protein aggregation is not fully understood.
Results: Heparin contributes to the initial steps of fibrillation, whereas protofibrillar intermediates accumulate transiently.
Conclusion: Heparin is involved in nucleation, and the transient rod-like protofibrils are off-pathway species.
Significance: Understanding the kinetic role of heparin and the protofibrils has implications for the development of therapies for tauopathies.

The aggregation of the natively disordered protein, Tau, to form lesions called neurofibrillary tangles is a characteristic feature of several neurodegenerative tauopathies. The polyanion, heparin, is commonly used as an inducer in studies of Tau aggregation *in vitro*, but there is surprisingly no comprehensive model describing, quantitatively, all aspects of the heparin-induced aggregation reaction. In this study, rate constants and extents of fibril formation by the four repeat domain of Tau (Tau4RD) have been reproducibly determined over a full range of heparin and protein concentrations. The kinetic role of heparin in the nucleation-dependent fibril formation reaction is shown to be limited to participation in the initial rate-limiting steps; a single heparin molecule binds two Tau4RD molecules, forming an aggregation-competent protein dimer, which then serves as a building block for further fibril growth. Importantly, the minimal kinetic model that is proposed can quantitatively account for the characteristic bell-shaped dependence of the aggregation kinetics on the stoichiometry of protein to heparin. Very importantly, this study also identifies for the first time short and thin, rod-like protofibrils that are populated transiently, early during the time course of fibril formation. The identification of these protofibrils as *bona fide* off-pathway species has implications for the development of therapies for tauopathies based on driving fibril formation as a means of protecting the cell from smaller, putatively toxic aggregates.

Tau is a microtubule-associated protein that is involved in microtubule stabilization and neurite outgrowth (1). In the adult human central nervous system, Tau exists in the form of six alternatively spliced isoforms; these isoforms differ by having three or four repeats in the C-terminal region, and zero, one, or two inserts in the N-terminal region (2, 3). The 31–32-residue-long pseudo-repeats in the C-terminal region together with the flanking proline-rich regions constitute the microtubule binding domain (4). In solution, Tau behaves as a random coil as judged by several tools, spectroscopic and otherwise, and hence belongs to the class of intrinsically unordered proteins (5–7).

The abnormal aggregation of Tau into paired helical filaments (PHFs)[3] and straight filaments is a hallmark of Alzheimer disease (AD) and other neurodegenerative tauopathies (8, 9). Interestingly, in AD it has been seen that the degree of cognitive impairment correlates better with neurofibrillary tangles (NFTs) composed of Tau than with senile plaques composed of the Aβ peptide (10, 11). Nevertheless, although the familial forms of AD are found to be associated with mutations that affect Aβ levels, which therefore implicate it in the causation of disease (12), no such mutations have been seen in the Tau gene. Tau is found to be hyper-phosphorylated and aggregated into NFTs in AD (13). In all the other tauopathies, however, mutations in the Tau gene link it to the disease context (14).

Tau fibrils formed *in vitro* from recombinant protein closely resemble those isolated from AD-diseased brain (15). They also possess the characteristic cross-β motif that is a feature of all amyloid fibrils (16–18). It has also been shown that the repeat domain of Tau, which constitutes the protease-resistant core of the PHFs (19) and which forms *bona fide* PHFs *in vitro*, serves as an equally good model system for investigating the aggregation of Tau, and its faster aggregation time scales make it more amenable for study (15, 20).

Although Tau dysfunction is implicated in neurodegeneration, the identity of the toxic aggregate remains unknown. For several other amyloid-related disorders, soluble oligomers and

* This work was funded by the Tata Institute of Fundamental Research and by the Department of Biotechnology, Government of India.
[S] The on-line version of this article (available at http://www.jbc.org) contains supplemental Methods, Equations 1 and 2, and Figs. 1–7.
[1] Recipient of the SP Mukherjee Fellowship from the Council of Scientific and Industrial Research, Government of India.
[2] Recipient of the JC Bose National Fellowship from the Government of India.
To whom correspondence should be addressed: National Centre for Biological Sciences, Tata Institute of Fundamental Research, Bangalore 560065, India. Tel.: 91-80-23666150; Fax: 91-80-23636662; E-mail: jayant@ncbs.res.in.

[3] The abbreviations used are: PHF, paired helical filament; NFT, neurofibrillary tangle; AD, Alzheimer disease; ThT, thioflavin T; AFM, atomic force microscopy; TEM, transmission electron microscopy; NDP, nucleation-dependent polymerization; P, protein; H, heparin.

protofibrils have been implicated as the toxic entities (21, 22). For Tau, the formation of canonical protofibrils has not been observed so far, although oligomers have been observed *in vitro* (23–25). Furthermore, except for one study (25), it is also not known whether these oligomers lie on or off the pathway of fibrillation. For other proteins, the evidence for on-pathway roles for oligomers and protofibrils is largely indirect (26, 27). An important goal of *in vitro* studies of the aggregation of Tau is to identify whether putatively toxic amyloid protofibrils are populated during the course of fibril formation and to determine whether they are on-pathway aggregates directly involved in fibril formation.

In vitro, amyloid fibril formation by Tau is extremely slow in the absence of polyanions, and the study of Tau aggregation becomes amenable only in the presence of polyanionic inducers that accelerate the reaction (28–35). In particular, the glycosaminoglycan heparin, whose structure closely mimics the highly sulfated regions of heparan sulfate, is commonly used to induce Tau aggregation *in vitro* (16, 17, 20, 23–25, 30–32, 35–47). Although Tau tangles are intracellular aggregates, they have been consistently found to contain components of the basement membrane such as heparan sulfate (48–51); it appears that this becomes possible during disease by mechanisms yet to be understood. Indeed, glycosaminoglycans such as heparan sulfate and other sulfated proteoglycans are also found in the amyloid deposits of many other proteins (52–54) even when the deposit is intracellular (55). Moreover, even though heparin is typically found outside the cell, the discovery that it, like other polyelectrolytes, can modulate amyloid fibril formation by many proteins (56–60) has led to its extensive use as a model for studying how other polyelectrolytes present within the cell, such as mRNA (61), might similarly affect amyloid fibril formation.

Nevertheless, the kinetic role of heparin in inducing the aggregation of Tau is not fully understood partly because there is still debate about whether polyanion-induced Tau aggregation into PHFs occurs by a nucleation-dependent polymerization (NDP) mechanism or not. An early pioneering study (20) utilizing artificially created Tau dimers suggested that an NDP mechanism operates and that heparin plays a role in the activation of Tau molecules leading to the formation of nucleation-competent oligomeric subunits. Similarly, studies with other inducers have also suggested an NDP mechanism for Tau aggregation (28, 29, 62). But a more recent study has suggested that polyanion-induced (including heparin-induced) Tau aggregation occurs not through a NDP mechanism but through essentially a downhill polymerization mechanism (30) in which heparin allosterically regulates conformational change into aggregation-competent subunits. Clearly, fundamental aspects of the heparin-induced aggregation reaction remain unresolved.

In this study the kinetics of amyloid fibril formation by the four repeat domain of Tau (Tau4RD) has been investigated in the presence of heparin at pH 7 and at 37 °C using thioflavin T (ThT) fluorescence as the probe. The kinetics is highly reproducible in the buffer conditions chosen, and AFM and TEM studies show that paired helical filaments as well as straight filaments are formed. In the minimal kinetic model proposed, which quantitatively describes all aspects of the aggregation reaction, heparin participates in the rate-limiting step of aggregation, with each heparin molecule binding sequentially to two Tau4RD molecules, leading to the formation of an aggregation-competent Tau dimer. Subsequent growth of fibrils appears to occur by stepwise addition of monomer protein. The minimal model quantitatively explains all aspects of the unusual dependence of aggregation kinetics on protein and heparin concentrations. Very importantly, this study also identifies for the first time rod-like protofibrillar forms around ~50 nm in length and ~2.6 nm in diameter, as measured by AFM, that are populated transiently during the aggregation reaction.

EXPERIMENTAL PROCEDURES

Protein Expression, Purification, and Characterization—The pET22b plasmid containing the Tau4RD gene (pETTau4RPH) was a kind gift from Prof. Takashi Konno (63). The protein is 144 amino acids long, spans the four repeats (Gln-244—Phe-378) of the longest isoform hTau40, and has a His tag at the C terminus and an isoelectric point of 9.68. The full amino acid sequence of the protein is as follows: MQTAPVPMPDLKNV-KSKIGSTENLKHQPGGGKVQIINKKLDLSNVQSKCGSKD-NIKHVPGGGSVQIVYKPVDLSKVTSKCGSLGNIHHKPGG-GQVEVKSEKLDFKDRVQSKIGSLDNITHVPGGGNKKIET-HKLTFLEHHHHHH. It is to be noted that His-tagged constructs of the protein have also been used in previous studies of the aggregation of the repeat domain as well as full-length Tau (33, 34, 63) and in a previous comparison of the aggregation of Tau constructs with and without a His tag, when induced by arachidonic acid, it was reported that the aggregation mechanism is not affected by the presence of the His tag (33).

The protocol that was standardized for Tau4RD purification is a slight modification of published protocols (64, 65) and makes use of cation-exchange chromatography followed by size-exclusion chromatography to obtain >99% pure protein and an average yield of ~100 mg/liter. A more detailed protocol is described in the supplemental Methods. The purity of the protein was confirmed by SDS-PAGE and electrospray ionization-MS. The mass of the protein was the expected 15,607 Da when determined using a Waters Q-TOF Ultima mass spectrometer.

Absorbance, fluorescence, and CD spectra were acquired to confirm spectroscopic signatures of the purified protein. The molar extinction coefficient of the protein at 280 nm was determined by the BCA assay (kit from Thermo Scientific) using bovine serum albumin as a standard and was found to be 1221 $M^{-1}cm^{-1}$. A dynamic light scattering experiment was performed to check that the purified protein was monomeric with the expected hydrodynamic radius (R_H) (40). The activity of the protein was determined using a tubulin polymerization assay monitored by turbidity measurements at 340 nm and at 37 °C as described earlier (4, 66). The activity was found to be reproducible across different protein preparations and better than that reported in the literature for proteins purified using a boiling lysis method (4).

Buffers, Solutions, and Experimental Conditions—All reagents used for experiments were of the highest purity grade available from Sigma unless otherwise specified. For the studies

involving aggregation in Tris buffer at pH 7, the protein stored in 25 mM Tris buffer, pH 7, was diluted into the aggregation buffer (25 mM Tris buffer, 1 mM DTT, pH 7) to the desired concentration. The desired concentration of NaCl (0–150 mM) was added to the aggregation buffer from a concentrated stock solution (2 M NaCl). For the experiment performed in Tris buffer at pH 7.5, a desired volume of a 1 M Tris buffer, pH 8.0, stock was added to the aggregation buffer described above, such that the final pH was 7.5, whereas the buffer strength remained unchanged. After dilution into the aggregation buffer, the protein was incubated for 2 h at 37 °C to allow for the reduction of any covalent Tau dimers to monomers. The reaction was then induced by the addition of heparin (M_r 12,000, Himedia Laboratories) of the desired concentration. The final pH remained unchanged, and the aggregation reaction continued to be maintained at 37 °C. The same heating block was used for all the experiments to reduce variability. Aggregation was also carried out in PBS buffer (pH 7.4) and this is described in the supplemental methods.

Typically, the volume of the aggregating protein solution was 1.5 ml. At different time points of aggregation, 5–100-μl aliquots of the protein sample were withdrawn, depending on the protein concentration being studied, for analysis by ThT fluorescence and AFM. Before removing a sample aliquot, the aggregating mixture was mixed three times with a P200 pipette. Great care was taken to ensure that there was no variation in the mixing technique every time an aliquot had to be removed so that the kinetics were fully reproducible, as the addition of heparin to the protein resulted in immediate turbidity and the formation of insoluble material that settled at the bottom of the tubes.

ThT Fluorescence Assay—The ThT assay was performed at pH 7 in 25 mM Tris buffer for the Tris aggregation reactions and at pH 7.4 in PBS for the PBS aggregation reactions. For the assay, a final concentration of 1 μM protein and 10 μM ThT was used. For every reading a calculated amount of the protein according to the concentration used in the aggregation experiment was withdrawn from the sample and added to the ThT assay solution. Measurements were made using a Fluoromax-3 spectrofluorimeter (Jobin Yvon) as described earlier (67).

Sedimentation Assay—The extent of amyloid fibril formation at the end of the aggregation reaction at a time corresponding to five time constants of the ThT fluorescence-monitored kinetics was determined by centrifugation of the solution at 20,000 × *g* for 45 min upon which the fibrils formed were found to have sedimented down. The sediment was insoluble in water but soluble in 6 M guanidine HCl. The amount of protein present in the sediment was determined by measurement of the Tyr fluorescence at 303 nm of sediment dissolved in 6 M guanidine HCl. To determine equilibrium monomer concentrations, the supernatant was passed through an YM100 Centricon (Millipore) to remove residual, soluble fibrils, and the Tyr fluorescence of the monomeric filtrate was measured.

Atomic Force Microscopy (AFM)—AFM samples of fibrils and protofibrils were made at specified times of aggregation and for fibrils, also at times corresponding to five time constants (5τ) of the ThT fluorescence-monitored kinetics.

For preparing samples, a 100-μl neat aliquot of the sample was withdrawn at the designated time, applied onto freshly cleaved mica (Grade V1, SPI Supplies), and allowed to incubate for 2 min in the case of fibril samples and 5 min in the case of protofibril samples. The mica surface was then rinsed with 25 drops of filtered MilliQ water and dried under vacuum for 1 h. AFM images were obtained on a PicoPlus AFM instrument (Molecular Imaging, Inc.) operating in the non-contact mode using 75 kHz, 2.8 newton/m cantilevers with a rounding tip radius of <10 nm (Nanoworld AG). Details of acquisition parameters are described in the supplemental Methods.

The diameters of the fibrils and protofibrils were determined by measuring the Z-heights of the structures in the AFM images (assuming them to be spherical or cylindrical) using the profile option of the program WSxM (68). Details of the analysis are described in the supplemental Methods.

TEM—A protein solution diluted to 5 μM was placed on a freshly glow-discharged, 400 mesh carbon-coated copper grid (Ted Pella) for 1 min, washed twice with filtered MilliQ water for 45 s, and then stained with 2% uranyl acetate for 30 s. After air-drying, the grids were examined on a Tecnai G^2 12 BioTwin electron microscope (FEI Co.) operating at 100 kV and equipped with a Gatan side mount 4k camera. Images were analyzed using the Gatan Digital Image micrograph software (Version 1.8).

Data Analysis—For the aggregation reactions in Tris buffer, the kinetic curves measured by ThT fluorescence were fitted to the single exponential equation,

$$S = S_0 + a[1 - e^{(-t/\tau)}] \quad \text{(Eq. 1)}$$

where S_0 is the signal at $t = 0$, t is the time, a is the amplitude of the signal change, and τ represents the time constant of aggregation.

RESULTS

Formation of Amyloid Fibrils by Tau in the Presence of Heparin—In this study amyloid fibril formation by the four repeat domain of Tau (Tau4RD) in the presence of heparin (M_r 12,000) has been studied in 25 mM Tris buffer at pH 7. Evidence for the formation of fibrils is provided by ThT binding (Fig. 1*a*), FTIR spectroscopy (supplemental Fig. 2*a*), and AFM (supplemental Fig. 2*b*). When monitored by ThT fluorescence, aggregation in Tris buffer appears to follow single-exponential kinetics with no lag phase at pH 7 (Fig. 1*a*) as well as at pH 7.5 (Fig. 1*a*, *inset*) and both in the absence of NaCl and in the presence of 25–150 mM NaCl (data not shown). Importantly, the kinetics of aggregation in Tris buffer is highly reproducible, as seen in the small spread in the data (Fig. 1*a*) even across different protein preparations. The high reproducibility of the data is because of the care taken to ensure that the starting preparation was free of seeds and was as homogeneous as possible. Before the addition of heparin, Tau4RD exists as a monomer with the expected (6, 40) hydrodynamic radius (R_H) of ~3 nm, as determined by dynamic light scattering (data not shown), and exists as a random coil as evident from its CD spectrum (data not shown). The high reproducibility of the data in Tris buffer made it possible to carry out a rigorous study of the kinetics of fibril formation in that buffer.

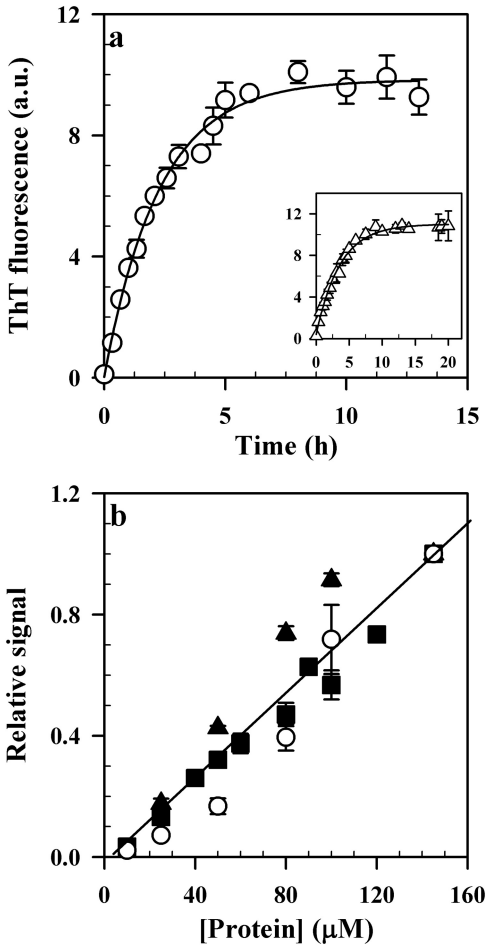

FIGURE 1. **Formation of amyloid fibrils by Tau4RD in the presence of heparin monitored by multiple probes.** *a*, ThT fluorescence monitored kinetics of 50 μM Tau4RD in the presence of 37.5 μM heparin at 37 °C in 25 mM Tris buffer, 50 mM NaCl, 1 mM DTT, pH 7. The *inset* shows a plot of ThT fluorescence-monitored kinetics in 25 mM Tris buffer, 50 mM NaCl, 1 mM DTT, pH 7.5. The continuous line through the data points in the main figure and in the *inset* is a least square fit to a single-exponential equation. The *error bars* represent the spread in the data calculated from two or more independent experiments and across different protein preparations. *a.u.*, arbitrary units. *b*, the extent of amyloid fibril formation at the end of the aggregation reaction is linear with respect to protein concentration as monitored by ThT fluorescence (■), light scattering at 800 nm (○), and a sedimentation assay (▲). The continuous line through the data points was drawn by inspection.

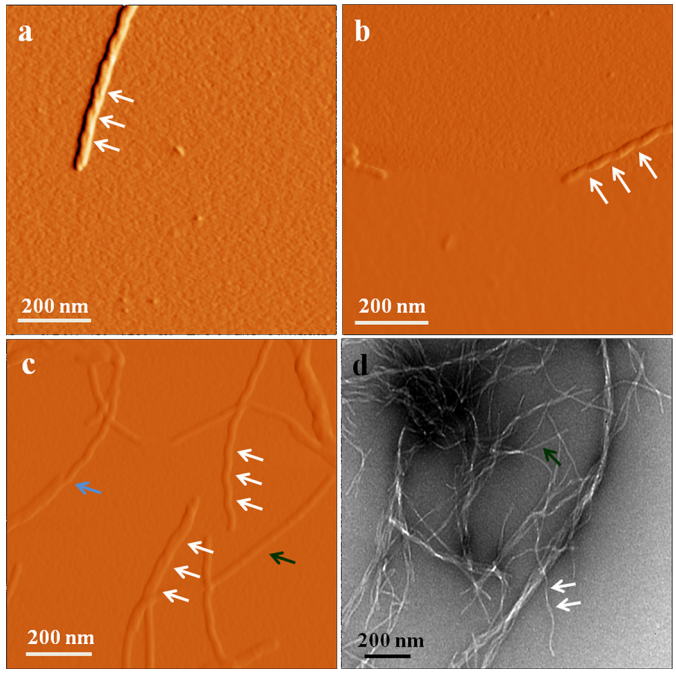

FIGURE 2. **Tau4RD forms a mixture of structures including characteristic PHFs in the presence of heparin in Tris buffer, pH 7, at 37 °C.** *a–c*, AFM images in the amplitude format of PHFs formed by 50 μM Tau4RD in the presence of 37.5 μM heparin display the expected cross-over repeat of ~80 nm as indicated by the *white arrows*. The *green arrow* in *c* point to a straight filament. The *blue arrow* in *c* points to an instance of a single filament emerging from a multi-stranded fibril. *d*, negatively stained TEM image of fibrils formed in the same conditions. The *white arrows* point to a PHF, and the *green arrow* points to a straight filament. The *scale bar* in all images corresponds to 200 nm. The Z scale for all AFM images corresponds to 8 nm.

In contrast, the aggregation kinetics in PBS buffer at pH 7.4 was found to be sigmoidal in nature in accordance with previous observations (32), displayed a final amplitude of ThT fluorescence at saturation that was almost 10-fold lower than that seen for aggregation in the Tris buffer, and was found to be not reproducible in terms of displaying a variable amplitude across protein preparations (supplemental Fig. 1*a*). Interestingly, the fibrils formed in the PBS and Tris buffers appear to have similar external morphologies as seen in AFM even though they appear to have different internal structures as monitored by FTIR spectroscopy (supplemental text and Fig. 2). In the future it will be important to determine by using high resolution probes such as hydrogen exchange NMR and solid-state NMR (69, 70) whether the fibrils formed in the two buffers do indeed differ in their internal structures (71).

In this study aggregation kinetics were studied over a range of protein and heparin concentrations using ThT fluorescence as the quantitative measure of the formation of structured, amyloid aggregates (72–76). The extent of fibril formation at any protein concentration was found to be the same whether monitored by ThT fluorescence, light scattering at 800 nm, or by direct measurement of the amount of fibrils formed using a sedimentation assay (Fig. 1*b*).

The Amyloid Fibrils Formed Include Characteristic PHFs—Because this is the first study of Tau aggregation in Tris pH 7 buffer, it was important to verify that the fibrils formed have the morphologies expected for Tau fibrils. AFM images show two kinds of structures, a twisted ribbon-like fibril previously described as a PHF and a flat ribbon-like fibril previously described as a straight filament. The PHFs appear to have a cross-over repeat of 80–100 nm and a maximal height of 10 nm, in accordance with previous observations (77). As also observed earlier (77, 78), two types of PHFs are seen; one in which two filaments appear to be wound around each other (Fig. 2*a*) and another that appears to be a single twisted ribbon (Fig. 2*b*). Other kinds of fibril morphologies are also seen (79). The twisted ribbon in Fig. 2*c* has a height of ~6 nm and a cross-over repeat of ~80–100 nm, whereas in the same field of view, a straight filament with a height of ~5 nm is also seen (Fig. 2*c*, *green arrow*).

The straight filaments and PHFs are also seen in a negatively stained TEM image of the fibrils (Fig. 2*d*). The average width of the straight filaments calculated from the TEM image (~10 nm) matches the average height of fibrils calculated from the AFM images, whereas the PHFs appear to have widths alternat-

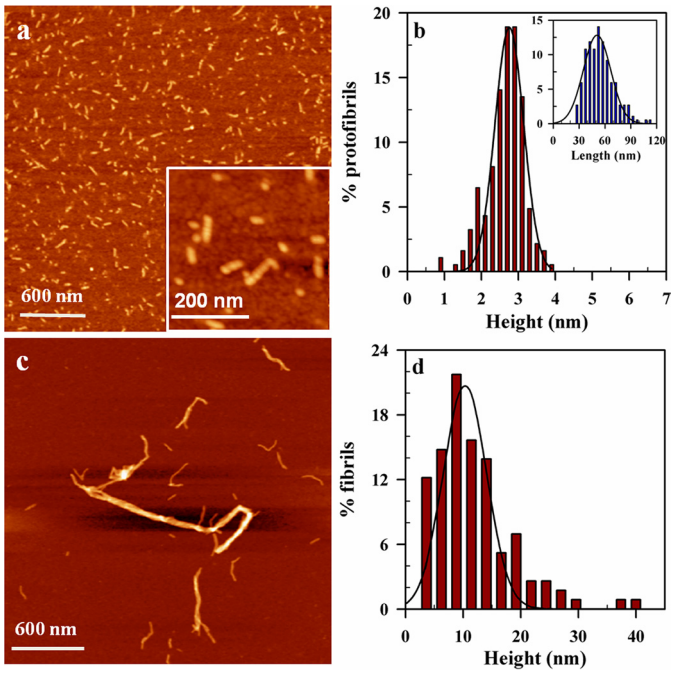

FIGURE 3. **Formation of protofibrils and fibrils by 50 μM Tau4RD in the presence of 37.5 μM heparin in Tris buffer, pH 7, at 37 °C.** *a*, an AFM image demonstrates the presence of short, rod-like protofibrils at 1 h of aggregation. The *inset* shows the beaded appearance of the protofibrils. The *scale bar* for the image corresponds to 600 nm, whereas that for the *inset* corresponds to 200 nm. The Z scale for the image corresponds to 8 nm, and that for the *inset* corresponds to 15 nm. *b*, distribution of heights of protofibrils is shown. The mean height calculated from the fit is 2.6 ± 0.5 nm. The *inset* shows the length distribution of the protofibrils is shown. The mean length calculated from the fit is 51 ± 16 nm. The *solid line* in both the image and the *inset* represents a fit to a Gaussian equation. *c*, an AFM image demonstrates the presence of fibrils at 1 h of aggregation. The *scale bar* for the image corresponds to 600 nm. The Z scale for the image corresponds to 50 nm. *d*, distribution of heights of fibrils is shown. The mean height calculated from the fit is 10.2 ± 3.9 nm. The *solid line* represents a fit to a Gaussian equation.

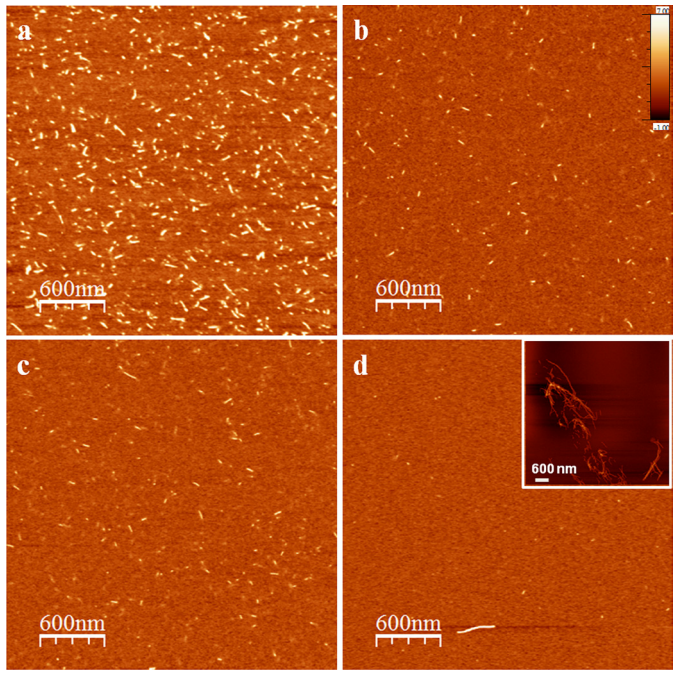

FIGURE 4. **The appearance and disappearance of protofibrils when 50 μM Tau4RD is aggregated in the presence of 37.5 μM heparin in Tris buffer, pH 7, at 37 °C.** *a–c*, AFM images of protofibrils at 20 min, 40 min, and 1 h of aggregation are shown. *d*, an AFM image demonstrates the absence of protofibrils at 2 h of aggregation. The *inset* is an image demonstrating the presence of fibrils at the same time point. The *scale bar* in all images as well as the *inset* corresponds to 600 nm. The Z scale for the main images corresponds to 8 nm, and the color scale applies to the main images. The Z scale for the *inset* corresponds to 50 nm.

ing between 9 and 16 nm, again with a cross-over repeat of ~80 nm (78).

When AFM images are acquired at very early times of aggregation (<20 min), large non-fibrillar aggregates are seen. These non-fibrillar aggregates sediment down upon centrifugation, as do the fibrillar aggregates. Unlike the fibrillar aggregates, the non-fibrillar aggregates appear to be water-soluble, and the relative fraction of sediment that is water-soluble decreases with time of aggregation (data not shown). Such nonspecific aggregates have also been found to accumulate transiently during the course of fibril formation by other proteins (80–82). The non-fibrillar aggregates are not seen in AFM images acquired at later times of aggregation (Figs. 2 and 3, supplemental Figs. 2–4). At the end of the fibril formation reaction, the sedimentation assay indicates that 95 ± 3% of the protein is present as water-insoluble, but denaturant-soluble aggregate and only fibrillar aggregates are observed by AFM (Fig. 2, supplemental Figs. 2–4). It, therefore, appears that the nonspecific aggregates formed at early times break down to monomer and transform into amyloid aggregates.

Protofibrils Are Transiently Populated during the Aggregation of Tau4RD in the Presence of Heparin—Fig. 3*a* demonstrates the existence of a distinct population of protofibrils captured at 1 h of aggregation. These short, rod-like protofibrils possess a mean height of 2.6 nm (Fig. 3*b*) and an average length of 50 nm (Fig. 3*b*, *inset*), and they also appear to be beaded (Fig. 3*a*, *inset*). Fibrils with an average height of 10.2 nm are also seen at the same time point of aggregation (Fig. 3, *c* and *d*). The protofibrils, however, constitute a population that is distinct from the fibrils both in terms of their lengths and their heights. Their characteristic height makes it easy to rule out the possibility that they may be fibril fragments of shorter length.

Fig. 4 shows AFM images acquired at four different times of aggregation of 50 μM Tau4RD in the presence of 37.5 μM heparin, which demonstrate the transient nature of the protofibrillar population. Although protofibrils are visible from 20 min to 1 h of aggregation (Fig. 4, *a–c*), they are, surprisingly, not visible at later times when probed by AFM. This pattern was seen reproducibly in three independent experiments, although there was variability in the density of the protofibrillar population that stuck to the mica across different experiments (as evident while comparing Figs. 3*a* and 4*c*).

At 1 h of aggregation, protofibrils and fibrils are seen in AFM images (Fig. 3); at 2 h, no protofibrils and only fibrils (Fig. 4*d*) are seen. Fibrils become longer from 1 h when protofibrils were last seen (Fig. 3*c*) to the end of the reaction (supplemental Figs. 2*b* and 3*b*; see the *insets* also), and this difference is visible by AFM. The height distribution of the few fibrils seen at the 1 h time point, when protofibrils are last seen, spans the entire range of heights seen at the end of the aggregation process (Fig. 3*d* and supplemental Fig. 3*e*). Thus, the fibrils do not signifi-

cantly increase in thickness from 1 h onward but do appear to increase in length.

Fibrillation of Tau4RD Is Sensitive to the Concentration of Heparin Present in the Buffer—The single exponential nature of the kinetics of aggregation is observed at all heparin concentrations (Fig. 5*a*). Heparin accelerates the apparent rate of fibril formation at low concentrations; this result is consistent with previous results (20, 30–32, 35, 36, 45, 47). Above ~25 μM heparin, the apparent rate decreases with a further increase in heparin concentration. Hence, the apparent rate of fibril formation displays a bell-shaped dependence on heparin concentration (Fig. 5*b*).

Interestingly, the amplitude of the change in ThT fluorescence displays a hyperbolic dependence on heparin concentration (Fig. 5*c*). Because the binding of heparin to Tau is tight, with a dissociation constant in the sub-micromolar region (44, 45), the hyperbolic dependence of the extent of fibril formation on heparin concentration (Fig. 5*c*) can be used to estimate reliably the stoichiometry of protein bound to heparin in the rate-limiting steps of aggregation; one heparin molecule appears to bind only 2–3 protein molecules.

Fibril Formation by Tau4RD in the Presence of Heparin Is Sensitive to Protein Concentration—The ThT fluorescence-monitored aggregation kinetics in the presence of 37.5 μM heparin are single-exponential at all protein concentrations (Fig. 6*a*), and the apparent rate constant shows a bell-shaped dependence on protein concentration (Figs. 6*b* and 5*b*) that peaks at a protein concentration of ~75–80 μM.

The amplitude of the change in the ThT signal has a linear dependence on protein concentration in the range of protein concentrations where the apparent rate constant increases and then decreases (Figs. 1*b* and 6*c*), but at very high protein concentrations the ThT fluorescence signal does reach a limiting value (Fig. 6*c*). The dissociation constant for Tau bound to heparin is less than 1 μM (44, 45). Hence, when the binding of protein to heparin, as monitored by the amplitude of ThT fluorescence change accompanying the aggregation reaction, is carried out at protein concentrations greatly exceeding the dissociation constant, the binding curve yields not the dissociation constant but only the stoichiometry of protein bound to heparin (83). Fig. 6*c* indicates, therefore, that only 1 heparin molecule is bound to 20 protein molecules when fibril formation is complete.

Fig. 6*c* also reveals that there exists a critical protein concentration below which Tau does not form fibrils. Linear regression analysis of the data in Fig. 6*c* provides a value of 5.0 ± 2.1 μM for the critical concentration; similar regression analysis of the rate constant dependence on Tau concentration (for the four lowest protein concentrations) (Fig. 6*b*) provides a value of 2.4 ± 0.5 μM. In confirmation of a critical concentration below which Tau does not aggregate, it was found that at protein concentrations of 2 and 3 μM, no increase in ThT fluorescence was seen even at 100 h, indicating that aggregation does not occur at these protein concentrations (data not shown). To further confirm the existence of a critical concentration, the solution at the end (five time constants) of the fibrillation reactions of 25, 50, and 100 μM protein was centrifuged at 20,000 × *g* for 45 min. It was found (data not shown, see "Experimental Procedures"), that the supernatant solutions in each case still contained 1 ± 0.5 μM protein, as expected if the critical concentration for aggregation is in the range of 1–3 μM.

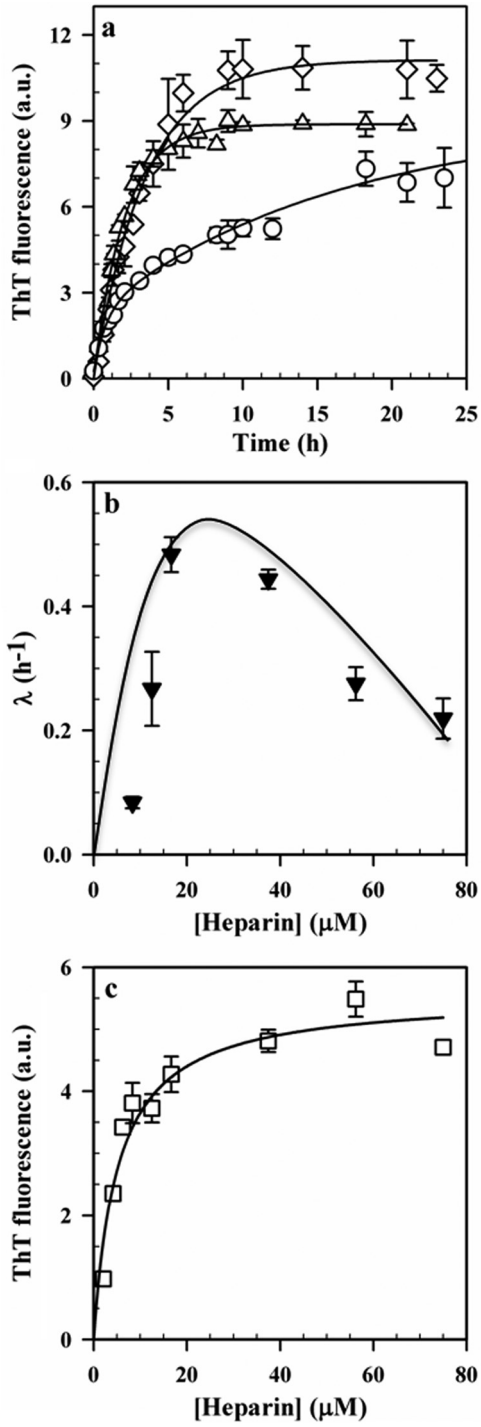

FIGURE 5. **Dependence on heparin concentration of ThT fluorescence-monitored kinetics in Tris buffer, pH 7.** *a*, kinetics of fibril formation by 50 μM Tau4RD in the presence of 8.3 μM (○), 16.6 μM (△), and 56.2 μM (◇) heparin are shown. The *continuous lines through the data points* are least-squares fits to a single-exponential equation. *a.u.*, arbitrary units. *b*, the apparent rate constant of ThT-monitored kinetics is plotted against heparin concentration. *c*, the amplitude of change in ThT fluorescence is plotted against heparin concentration. The *error bars* in *a*–*c* represent the spread in the data calculated from two or more independent experiments and across protein preparations. The *continuous lines through the data points* in *b* and *c* were drawn by inspection to guide the eye.

Fibril Formation by Tau4RD in the Presence of Heparin Depends on the Stoichiometry of the Two Partners—The bell-shaped dependence of the fibrillation rate constants on both

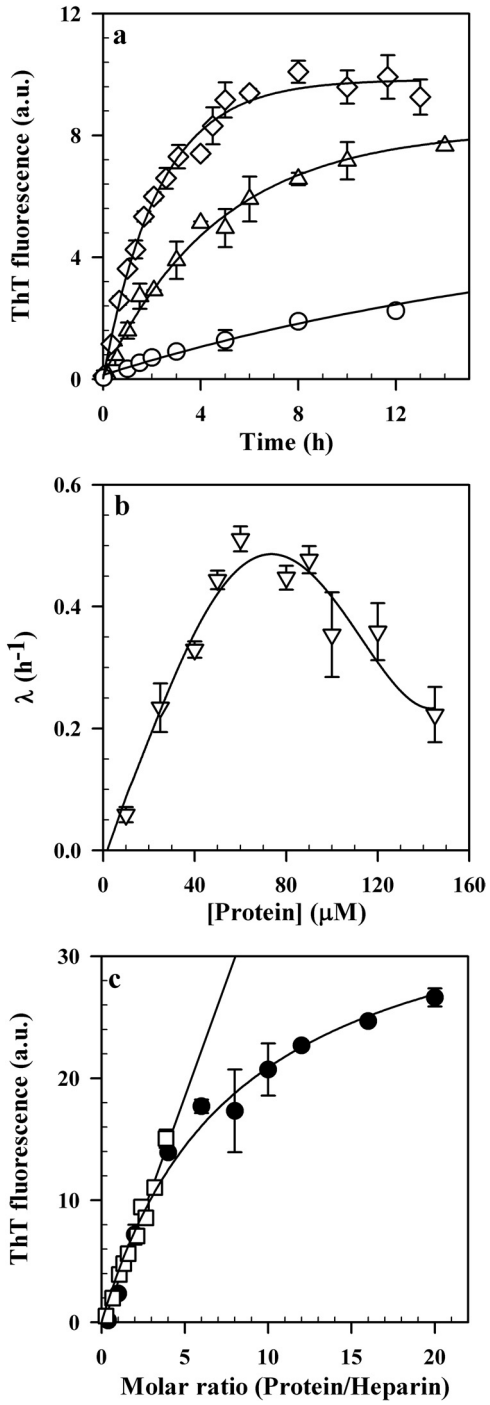

FIGURE 6. **Dependence on protein concentration of ThT fluorescence-monitored kinetics in Tris buffer, pH 7.** *a*, kinetics of fibril formation by 10 μM (○), 25 μM (△) and 50 μM Tau4RD (◇) in the presence of 37.5 μM heparin are shown. *The continuous lines through the data points* represent least-squares fits to a single-exponential equation. *a.u.*, arbitrary units. *b*, the apparent rate constant of ThT-monitored kinetics is plotted against protein concentration. The *continuous line through the data points* was drawn by inspection. *c*, the amplitude of the change in ThT fluorescence when protein is added to 5 μM heparin (●) and when protein is added to 37.5 μM heparin (□) as a function of the molar ratio of protein:heparin is shown. The *straight line through the data points* is a least-square fit. The *continuous line through the data points* was drawn by inspection to guide the eye. The *error bars* in *a–c* represent the spread in the data calculated from two or more independent experiments.

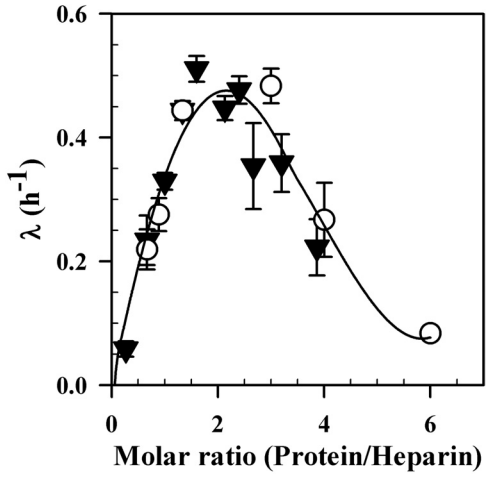

FIGURE 7. **Dependence of the apparent rate constant of ThT fluorescence-monitored kinetics on the molar ratio of protein to heparin.** The apparent rate constant of fibril formation is plotted as a function of molar ratio from aggregation experiments wherein the protein concentration is held constant and the heparin concentration is varied (*white symbols*) and wherein the heparin concentration is held constant and the protein concentration is varied (*black symbols*).

heparin and protein concentration are coincident when the rate constants are plotted against the molar ratio of protein to heparin, and the peak of this bell-shaped pattern lies at a ratio of ~2 (Fig. 7). When the molar ratio is kept fixed and the protein and heparin concentrations are varied accordingly, the rate remains the same, proving that the role of stoichiometry is not incidental but rather crucial to the aggregation process (data not shown).

Kinetic Simulations—The utility of kinetic simulations in determining protein aggregation mechanisms has been discussed (84, 85), and in this study kinetic simulations were carried out using the program Tenua, a variant of KINSIM (86), to determine the minimal model that describes all important features of the data. The model had to explain 1) the absence of a lag phase in the kinetics, 2) the bell-shaped dependence of the aggregation rate on heparin concentration, 3) the hyperbolic dependence of the extent of fibril formation on heparin concentration, 4) the bell-shaped dependence of the aggregation rate on protein concentration, 5) the linear dependence of the extent of fibril formation on protein concentration, and 6) the bell-shaped dependence of aggregation rate on the ratio of protein concentration to heparin concentration. Moreover the model needs to be consistent with the observation that nonspecific, non-fibrillar, and protofibrillar aggregates form transiently, early during aggregation.

Fig. 8 shows the simplest model that accounts for all the experimental data. In this model the critical role of heparin (H) is to enable the formation of the aggregation-competent dimer, which then acts as a nucleus for further growth. Elongation is shown to occur by a monomer addition mechanism, wherein individual protein molecules (P) add to the growing fibril, undergoing conformational conversion as they do so. The rate-limiting steps of this reaction are those involved in dimer formation; all subsequent growth steps are expected to be much faster and, hence, do not affect the overall aggregation rate. The model also shows a non-productive protein-heparin complex

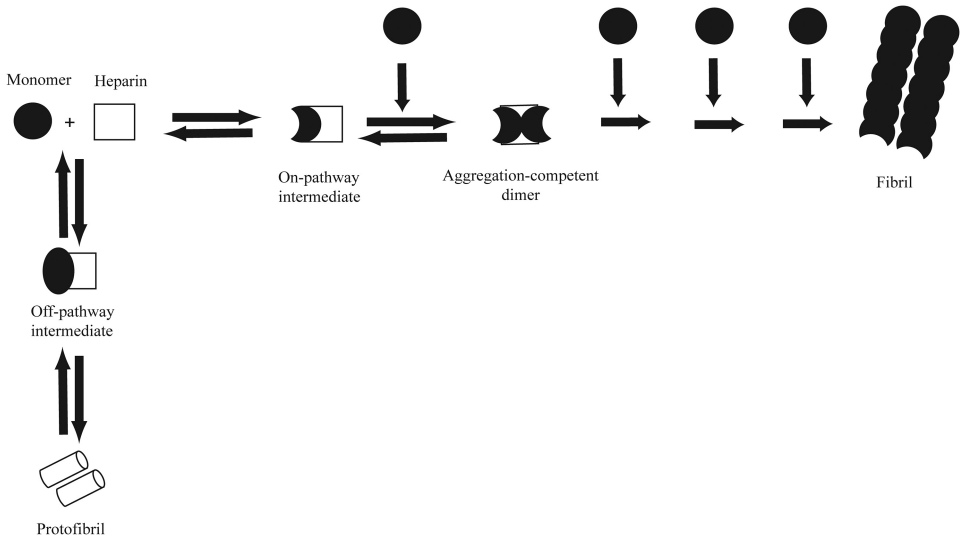

FIGURE 8. **Model for the formation of fibrils by the repeat domain of Tau in the presence of heparin.** Protein binds heparin and undergoes a conformational change to form an on-pathway intermediate, PH. When a second protein molecule binds the same heparin molecule, an aggregation-competent dimer (PHP) is formed. Elongation leading to fibril formation occurs by the process of monomer addition to this building block. An off-pathway intermediate in the form of a tight binding, P*H complex also forms and modulates the aggregation kinetics. It appears that this off-pathway intermediate can aggregate to form the rod-like protofibrils that are observed to accumulate transiently.

forming off-pathway to the main aggregation pathway. This off-pathway step accounts for the observation that fibril formation is slowed down at high protein concentrations.

Kinetic simulations (supplemental Figs. 6 and 7) show that this model satisfactorily explains all aspects of the experimental data described above. An important assumption of the simulations was that P in PH as well as in PHP is as capable of binding ThT as is P in the fibrils, which is consistent with previous results (87) that had indicated that initial monomeric intermediates formed during aggregation can bind ThT(S). It should be noted that the simulation has been carried out with the minimum number of aggregate growth steps necessary to account for the basic features of the data.

DISCUSSION

Mechanism of Heparin-induced Amyloid Fibril Formation by Tau—Heparin has been used extensively as an inducer in studies of Tau aggregation (16, 17, 20, 23–25, 30–32, 35–47), but only a few quantitative models (20, 30, 45) have been proposed to describe important aspects of amyloid fibril formation. However, even in these elegant models, the kinetic role of heparin either in activation, in nucleation, or in allosteric regulation was not quantitatively described as was not the unusual dependence of aggregation kinetics on both protein and heparin concentration (20, 30, 45). In this study a minimal kinetic model is presented that provides an intuitive description of important aspects of the data. Very importantly, numerical simulations based on this model are shown to quantitatively describe the dependence of the rate and extent of aggregation on protein and heparin concentrations.

The Aggregation Model Is Based on a NDP Mechanism—The mechanism of heparin-induced Tau aggregation has been conclusively described as NDP by only one previous study that made use of artificially created covalent Tau dimers (20). Other kinetic studies of heparin-induced Tau aggregation have data that are consistent with a NDP mechanism, but these data were not fitted to quantitative models of NDP (32, 45). An explicit description of the Tau fibrillation mechanism as NDP has been made only in studies that have examined the effect of inducers other than heparin (28, 29, 87) or used phosphorylated or truncated protein (88, 89), but even in these studies the unusual dependencies of aggregation kinetics on both protein and inducer concentrations were not quantitatively described.

Uncertainty about whether heparin-induced Tau aggregation follows a NDP mechanism had arisen because a recent study suggested that it follows instead an isodesmic (downhill) mechanism (30). However, in this as well as in other previous studies (20, 28, 29, 45, 62), both a dependence of aggregation rates on protein concentration and a critical concentration ($\sim$ 1–3 μM) are observed (see "Results"), as expected for a NDP mechanism but not for an isodesmic mechanism (84, 90, 91). The latter also seems unlikely because the morphology of Tau fibrils (Figs. 2 and 3 and supplemental Figs. 2–4) is not consistent with that of an isodesmic polymer, and moreover, progressively larger, small pre-fibrillar oligomers are not observed.

The minimal model shown in Fig. 8 is based on a ligand-induced NDP mechanism. The steps leading to the formation of a dimer are the slowest steps, and hence, the heparin-bound dimer functions as would a nucleus in a NDP mechanism. No lag phase in the aggregation kinetics is observable only because of the specific values of the rate constants defining the two nucleation steps (supplemental Fig. 6) in the Tris buffer system utilized in this study. Sigmoidal kinetics, typical of NDP (92, 93), are, however, seen in PBS buffer (supplemental Fig. 1*a*). Importantly, fibrils formed in the Tris buffer can function as seeds to eliminate the initial lag phase otherwise observed during aggregation in PBS buffer (data not shown).

The Minimal Model Describes the Dependence of the Aggregation Kinetics on Heparin Concentration—The observation that the ThT fluorescence saturates at a heparin concentration

approximately half that of the protein present (Fig. 5*c*) forms the basis of the model (Fig. 8) that a complex of one heparin molecule with two bound Tau molecules forms in the rate-limiting steps of aggregation. Heparin (H) brings two positively charged monomeric protein (P) molecules together, thus enabling them to interact and undergo the conformational change necessary to form the aggregation nucleus (PHP). Indeed, heparin has been shown to induce conformational changes in Tau (44, 46), and a role for heparin in regulating the conformation of Tau has been proposed earlier (30). It has also been postulated that heparin functions by binding sites of residual β structure and facilitating β-strand interactions across different Tau molecules (38). Indeed, two such hexapeptide motifs have been demonstrated to be minimal Tau-Tau interaction motifs that form PHFs *in vitro* (39).

An earlier study of the induction of Tau aggregation by the small molecule thiazine red had indicated that the rate-limiting step in fibril formation is dimerization (62), but in that study the aggregation rate was found to not depend on the stoichiometry of protein to inducer as it does, characteristically, for heparin-induced aggregation (31, 62). This is the first study to demonstrate, quantitatively, the kinetic role of an aggregation-competent non-covalent dimer in the mechanism of heparin-induced aggregation. Previous studies (20, 32, 47) of the aggregation of a covalently linked dimer of Tau had suggested, qualitatively, that covalent dimerization is important because of its effect in increasing the apparent rate of aggregation.

Thus, the minimal model (Fig. 8) is consistent with the observation that the apparent rate constant of fibril formation reaches its maximum value when the heparin concentration is half the protein concentration (Figs. 5 and 7). All protein molecules are then tightly bound to heparin molecules in PHP complexes, the concentration of PHP is at its maximum value, and the apparent rate of aggregation is at its maximum value. At higher concentrations of heparin, the apparent rate constant of fibril formation decreases because the PHP concentration begins to decrease from its maximum value when the free heparin concentration becomes much larger than the equilibrium constant for PH dissociation. A similar effect of polyanions has been observed on the folding of the dimeric Arc repressor (94).

Other explanations for the inhibitory action of heparin at high concentrations have been proposed. The explanation based on the existence of a low affinity binding site for heparin, binding to which at high heparin concentrations would reduce the concentration of the aggregation-competent PHP molecules, is plausible (31), especially as it is known that Tau has multiple heparin binding sites (44), but it requires a more complex model than the minimal model shown in Fig. 8. The explanation based on heparin exerting a Debye screening effect (45) is unlikely because even at the highest heparin concentration used in this study (75 μM), its contribution to the ionic strength would not exceed 7 mM, whereas the ionic strength effect on the apparent rate of fibril formation is seen at significantly higher NaCl concentrations (supplemental Fig. 1*b*).

The Minimal Model Describes the Dependence of the Aggregation Kinetics on Protein Concentration—The observation made in this study that the apparent rate constant for fibril formation increases with protein concentration and reaches its maximum value when the concentration of protein is twice that of the heparin present (Figs. 6 and 7) is accounted for by the minimal model (Fig. 8). Several previous studies had examined the effect of varying protein concentration and the effect of the molar ratio of Tau:heparin on Tau polymerization (20, 30, 31, 45). Although concluding that the stoichiometry of the two partners influences fibrillation, they could not explain the mechanistic basis for this dependence.

To account for the observation that the apparent rate of fibril formation then reduces with a further increase in protein concentration, the minimal model includes an additional process that is off-pathway to the pathway for the formation of the aggregation-competent dimer. In this off-pathway process, heparin binds to a tight binding site on each Tau molecule, much more tightly than it does to the site that leads to the formation of PH and PHP on the main aggregation pathway (Fig. 8 and supplemental Fig. 6). Binding of heparin to this tight binding site leads to the formation of the complex P*H, whose conformation is such that it is incapable of participating in the fibril formation reaction. This study, therefore, provides direct kinetic evidence in support of the insightful suggestion made several years ago that assembly-incompetent complexes of Tau and polyanion are also likely to form during the course of the aggregation reaction (20, 31).

An alternative off-pathway process that would also result in fibril formation becoming slower at high protein concentrations is one that would lead to the formation of an aggregation-incompetent dimer, PP, in a process that is not heparin-dependent and that is off the pathway for heparin-facilitated dimer formation. The binding constant for the formation of PP would have to be weak, so that it would form significantly only at high protein concentrations, thereby slowing down fibril formation. Indeed, it has been reported that Tau is capable of forming non-covalent dimers (32).

The Minimal Model and Fibril Growth—In the minimal model (Fig. 8), fibril growth occurs by monomer addition to the aggregation-competent dimer, and heparin is not assigned any role in fibril elongation. On the other hand, if elongation were to occur by linear addition of either PHP or PH, then the observations here (see below) and elsewhere (30, 43) that heparin is not an integral part of the fibril structure would require that heparin dissociate from the growing fibril once its role in elongation is over. This would happen, for example, if growth of the fibril is accompanied by conformational changes in the assembled Tau molecules, which lead to the dissociation of heparin from the fibrils. Such a possible role of heparin in fibril elongation cannot be ruled out in this study because it would be after the rate-limiting step.

There has been some debate about whether heparin is a major constituent of fibrils (30, 43, 44). The observation made in this study that the final fibrils contain less than one heparin molecule for every 20 protein molecules (see "Results") is the strongest evidence so far that heparin is only a minor constituent of fibrils. Indeed, an earlier study using radio-labeled heparin had also estimated that fibrils contained less than 1 heparin molecule for every 20 protein molecules (30). Not surprisingly then, neither the height distributions of fibrils, as determined by AFM (supplemental Figs. 3 and 4), nor their internal struc-

tures, as determined by FTIR spectroscopy (supplemental Fig. 5), are affected by the stoichiometry of protein to polyanion present during aggregation.

Protofibrils Are Transiently Populated during the Aggregation Process—A significant result of this study is the identification of short canonical protofibrils, ~2.6 nm thick and ~50 nm long, that are very transiently populated during the course of amyloid fibril formation (Figs. 3 and 4). They are beaded structures (Fig. 3*a*, *inset*), and in that sense, they are similar to the linear arrays of spherical nucleation units seen earlier (25). The rod-like protofibrils are, however, distinct from not only the spherical nucleation units and the granular Tau oligomers (23), both of which are large (>20 nm) structures formed by full-length recombinant hTau40 as fibrillation intermediates, but also from the soluble, heterogeneous oligomeric population formed by a C-terminal fragment of human Tau (24).

The observation that the rate of growth of fibrillar material as measured by ThT fluorescence (Fig. 1*a*) as well as the rate of increase in fibril length as observed by AFM (Fig. 3*c* and supplemental Figs. 2*b* and 3*b*; see insets also) is much slower than the rate of disappearance of the protofibrils (Fig. 4) suggests that the protofibrils are not direct precursors to fibril formation. Instead they accumulate off the main pathway of fibril formation but too transiently for either the extent or rate of their formation to be determined. The surprisingly fast rate at which they disappear suggests that they are unstable and, hence, are populated to a small extent. The minimal model (Fig. 8) can suggest how they may form in a process that is off the main pathway for fibril formation. The protofibrils could form rapidly and reversibly from P*H (Fig. 8, supplemental Fig. 6), which is formed much more rapidly than is PH on the main aggregation pathway. As PH undergoes further transformation into PHP and then into larger aggregates, thermodynamic linkage (95) leads to, at first, a reduction in the concentration of P, which is then replenished at the cost of a reduction in the concentration of P*H. Ultimately, linkage would lead to the dissociation of the protofibrils into P*H, whose rate appears to be rapid.

To demonstrate that the rod-like protofibrils also form *in vivo* is an important goal of future studies, made difficult both by their small (suboptical resolution) size and by their ephemeral existence. Nevertheless, their identification *in vitro* suggests new ways in which Tau might behave in neurons in the normal state or when the normal state is perturbed. Indeed, the discovery that Tau can form protofibrils under near-physiological conditions *in vitro* highlights the importance of *in vitro* studies. Because *in vivo* conditions may be very different in the normal and diseased state, *in vitro* studies can suggest ways in which the biochemical system may adapt upon such change.

Physiological Relevance of This Study—This study is important from two perspectives. First, the quantitative demonstration that the glycosaminoglycan heparin plays a role in only the nucleation steps and not the elongation steps of Tau aggregation *in vitro* implies that very small amounts of heparin would be capable of triggering Tau fibrillation *in vivo*. This is important from the perspective of understanding tauopathies because, although glycosaminoglycans have been detected in NFTs in various tauopathies (48–51, 96) and have been detected in nerve cells at early stages of neurodegeneration (8, 35, 97), their role in Tau aggregation and disease progression has eluded proper understanding. Second and importantly, the observation made here for the first time that Tau can form protofibrils similar in morphology to those formed by other proteins (98–100) has important implications for the control of disease progression in tauopathies. If Tau protofibrils also turn out to be toxic like other protofibrils (21, 101), then their identification in this study as off-pathway species has important implications for the development of therapies based on driving NFT formation as a means to remove the soluble, toxic protofibrils from the cytoplasm. The identification of putatively toxic Tau protofibrils is especially important in the context of *in vivo* studies that have indicated that cognitive deficits and cell death are unrelated to NFT accumulation (102–104) and that Tau oligomers, and not fibrils, impair memory and induce synaptic dysfunction (105). In future studies it will be important to study the toxicity of the protofibrils and whether compounds that inhibit Tau fibril formation (106, 107) also affect the extent of protofibril formation.

Acknowledgments—We thank members of our laboratory for discussion and comments on the manuscript. We thank Prof. R. Varadarajan for discussions, Dr. B. Shivu for assistance with the Thin Film-ATR FTIR technique, and Prof. G. Krishnamoorthy for help with the initial AFM measurements. The TEM and AFM images were collected at the Central Imaging Facility of the National Centre for Biological Sciences, and the mass spectra were collected at the Mass Spectrometry Facility of the National Centre for Biological Sciences.

REFERENCES

1. Weingarten, M. D., Lockwood, A. H., Hwo, S. Y., and Kirschner, M. W. (1975) *Proc. Natl. Acad. Sci. U.S.A.* **72,** 1858–1862
2. Goedert, M., Spillantini, M. G., Jakes, R., Rutherford, D., and Crowther, R. A. (1989) *Neuron* **3,** 519–526
3. Lee, G., Cowan, N., and Kirschner, M. (1988) *Science* **239,** 285–288
4. Gustke, N., Trinczek, B., Biernat, J., Mandelkow, E. M., and Mandelkow, E. (1994) *Biochemistry* **33,** 9511–9522
5. Schweers, O., Schönbrunn-Hanebeck, E., Marx, A., and Mandelkow, E. (1994) *J. Biol. Chem.* **269,** 24290–24297
6. Mylonas, E., Hascher, A., Bernadó, P., Blackledge, M., Mandelkow, E., and Svergun, D. I. (2008) *Biochemistry* **47,** 10345–10353
7. Mukrasch, M. D., Bibow, S., Korukottu, J., Jeganathan, S., Biernat, J., Griesinger, C., Mandelkow, E., and Zweckstetter, M. (2009) *PLoS Biol.* **7,** e34
8. Goedert, M., Spillantini, M. G., and Davies, S. W. (1998) *Curr. Opin. Neurobiol.* **8,** 619–632
9. Ballatore, C., Lee, V. M., and Trojanowski, J. Q. (2007) *Nat. Rev. Neurosci.* **8,** 663–672
10. Arriagada, P. V., Marzloff, K., and Hyman, B. T. (1992) *Neurology* **42,** 1681–1688
11. Wilcock, G. K., and Esiri, M. M. (1982) *J. Neurol. Sci.* **56,** 343–356
12. St George-Hyslop, P. H., and Petit, A. (2005) *C. R. Biol.* **328,** 119–130
13. Grundke-Iqbal, I., Iqbal, K., Tung, Y. C., Quinlan, M., Wisniewski, H. M., and Binder, L. I. (1986) *Proc. Natl. Acad. Sci. U.S.A.* **83,** 4913–4917
14. Garcia, M. L., and Cleveland, D. W. (2001) *Curr. Opin. Cell Biol.* **13,** 41–48
15. Wille, H., Drewes, G., Biernat, J., Mandelkow, E. M., and Mandelkow, E. (1992) *J. Cell Biol.* **118,** 573–584
16. Barghorn, S., Davies, P., and Mandelkow, E. (2004) *Biochemistry* **43,** 1694–1703
17. Berriman, J., Serpell, L. C., Oberg, K. A., Fink, A. L., Goedert, M., and

Crowther, R. A. (2003) *Proc. Natl. Acad. Sci. U.S.A.* **100,** 9034–9038
18. Inouye, H., Sharma, D., Goux, W. J., and Kirschner, D. A. (2006) *Biophys. J.* **90,** 1774–1789
19. Wischik, C. M., Novak, M., Edwards, P. C., Klug, A., Tichelaar, W., and Crowther, R. A. (1988) *Proc. Natl. Acad. Sci. U.S.A.* **85,** 4884–4888
20. Friedhoff, P., von Bergen, M., Mandelkow, E. M., Davies, P., and Mandelkow, E. (1998) *Proc. Natl. Acad. Sci. U.S.A.* **95,** 15712–15717
21. Caughey, B., and Lansbury, P. T. (2003) *Annu. Rev. Neurosci.* **26,** 267–298
22. Chiti, F., and Dobson, C. M. (2006) *Annu. Rev. Biochem.* **75,** 333–366
23. Maeda, S., Sahara, N., Saito, Y., Murayama, M., Yoshiike, Y., Kim, H., Miyasaka, T., Murayama, S., Ikai, A., and Takashima, A. (2007) *Biochemistry* **46,** 3856–3861
24. Peterson, D. W., Zhou, H., Dahlquist, F. W., and Lew, J. (2008) *Biochemistry* **47,** 7393–7404
25. Xu, S., Brunden, K. R., Trojanowski, J. Q., and Lee, V. M. (2010) *Alzheimers Dement.* **6,** 110–117
26. Kheterpal, I., Chen, M., Cook, K. D., and Wetzel, R. (2006) *J. Mol. Biol.* **361,** 785–795
27. Serio, T. R., Cashikar, A. G., Kowal, A. S., Sawicki, G. J., Moslehi, J. J., Serpell, L., Arnsdorf, M. F., and Lindquist, S. L. (2000) *Science* **289,** 1317–1321
28. King, M. E., Ahuja, V., Binder, L. I., and Kuret, J. (1999) *Biochemistry* **38,** 14851–14859
29. Chirita, C. N., Congdon, E. E., Yin, H., and Kuret, J. (2005) *Biochemistry* **44,** 5862–5872
30. Carlson, S. W., Branden, M., Voss, K., Sun, Q., Rankin, C. A., and Gamblin, T. C. (2007) *Biochemistry* **46,** 8838–8849
31. Friedhoff, P., Schneider, A., Mandelkow, E. M., and Mandelkow, E. (1998) *Biochemistry* **37,** 10223–10230
32. Barghorn, S., and Mandelkow, E. (2002) *Biochemistry* **41,** 14885–14896
33. King, M. E., Gamblin, T. C., Kuret, J., and Binder, L. I. (2000) *J. Neurochem.* **74,** 1749–1757
34. Chirita, C. N., Necula, M., and Kuret, J. (2003) *J. Biol. Chem.* **278,** 25644–25650
35. Goedert, M., Jakes, R., Spillantini, M. G., Hasegawa, M., Smith, M. J., and Crowther, R. A. (1996) *Nature* **383,** 550–553
36. Pérez, M., Valpuesta, J. M., Medina, M., Montejo de Garcini, E., and Avila, J. (1996) *J. Neurochem.* **67,** 1183–1190
37. Hasegawa, M., Crowther, R. A., Jakes, R., and Goedert, M. (1997) *J. Biol. Chem.* **272,** 33118–33124
38. Mukrasch, M. D., Biernat, J., von Bergen, M., Griesinger, C., Mandelkow, E., and Zweckstetter, M. (2005) *J. Biol. Chem.* **280,** 24978–24986
39. von Bergen, M., Friedhoff, P., Biernat, J., Heberle, J., Mandelkow, E. M., and Mandelkow, E. (2000) *Proc. Natl. Acad. Sci. U.S.A.* **97,** 5129–5134
40. Yao, T. M., Tomoo, K., Ishida, T., Hasegawa, H., Sasaki, M., and Taniguchi, T. (2003) *J. Biochem.* **134,** 91–99
41. Jeganathan, S., von Bergen, M., Mandelkow, E. M., and Mandelkow, E. (2008) *Biochemistry* **47,** 10526–10539
42. Andronesi, O. C., von Bergen, M., Biernat, J., Seidel, K., Griesinger, C., Mandelkow, E., and Baldus, M. (2008) *J. Am. Chem. Soc.* **130,** 5922–5928
43. von Bergen, M., Barghorn, S., Müller, S. A., Pickhardt, M., Biernat, J., Mandelkow, E. M., Davies, P., Aebi, U., and Mandelkow, E. (2006) *Biochemistry* **45,** 6446–6457
44. Sibille, N., Sillen, A., Leroy, A., Wieruszeski, J. M., Mulloy, B., Landrieu, I., and Lippens, G. (2006) *Biochemistry* **45,** 12560–12572
45. Zhu, H. L., Fernández, C., Fan, J. B., Shewmaker, F., Chen, J., Minton, A. P., and Liang, Y. (2010) *J. Biol. Chem.* **285,** 3592–3599
46. Paudel, H. K., and Li, W. (1999) *J. Biol. Chem.* **274,** 8029–8038
47. Schweers, O., Mandelkow, E. M., Biernat, J., and Mandelkow, E. (1995) *Proc. Natl. Acad. Sci. U.S.A.* **92,** 8463–8467
48. Perry, G., Siedlak, S. L., Richey, P., Kawai, M., Cras, P., Kalaria, R. N., Galloway, P. G., Scardina, J. M., Cordell, B., and Greenberg, B. D. (1991) *J. Neurosci.* **11,** 3679–3683
49. Snow, A. D., Mar, H., Nochlin, D., Kresse, H., and Wight, T. N. (1992) *J. Histochem. Cytochem.* **40,** 105–113
50. Su, J. H., Cummings, B. J., and Cotman, C. W. (1992) *Neuroscience* **51,** 801–813
51. DeWitt, D. A., Silver, J., Canning, D. R., and Perry, G. (1993) *Exp. Neurol.* **121,** 149–152
52. Magnus, J. H., Stenstad, T., Kolset, S. O., and Husby, G. (1991) *Scand. J. Immunol.* **34,** 63–69
53. Young, I. D., Willmer, J. P., and Kisilevsky, R. (1989) *Acta Neuropathol.* **78,** 202–209
54. Young, I. D., Ailles, L., Narindrasorasak, S., Tan, R., and Kisilevsky, R. (1992) *Arch. Pathol. Lab. Med.* **116,** 951–954
55. Cohlberg, J. A., Li, J., Uversky, V. N., and Fink, A. L. (2002) *Biochemistry* **41,** 1502–1511
56. Calamai, M., Kumita, J. R., Mifsud, J., Parrini, C., Ramazzotti, M., Ramponi, G., Taddei, N., Chiti, F., and Dobson, C. M. (2006) *Biochemistry* **45,** 12806–12815
57. Motamedi-Shad, N., Monsellier, E., Torrassa, S., Relini, A., and Chiti, F. (2009) *J. Biol. Chem.* **284,** 29921–29934
58. Suk, J. Y., Zhang, F., Balch, W. E., Linhardt, R. J., and Kelly, J. W. (2006) *Biochemistry* **45,** 2234–2242
59. Myers, S. L., Jones, S., Jahn, T. R., Morten, I. J., Tennent, G. A., Hewitt, E. W., and Radford, S. E. (2006) *Biochemistry* **45,** 2311–2321
60. Bazar, E., and Jelinek, R. (2010) *Chembiochem* **11,** 1997–2002
61. Ginsberg, S. D., Crino, P. B., Lee, V. M., Eberwine, J. H., and Trojanowski, J. Q. (1997) *Ann. Neurol.* **41,** 200–209
62. Congdon, E. E., Kim, S., Bonchak, J., Songrug, T., Matzavinos, A., and Kuret, J. (2008) *J. Biol. Chem.* **283,** 13806–13816
63. Konno, T., Oiki, S., Hasegawa, K., and Naiki, H. (2004) *Biochemistry* **43,** 13613–13620
64. Csokova, N., Skrabana, R., Liebig, H. D., Mederlyova, A., Kontsek, P., and Novak, M. (2004) *Protein Expr. Purif.* **35,** 366–372
65. Barghorn, S., Biernat, J., and Mandelkow, E. (2005) *Methods Mol. Biol.* **299,** 35–51
66. Kar, S., Fan, J., Smith, M. J., Goedert, M., and Amos, L. A. (2003) *EMBO J.* **22,** 70–77
67. Jain, S., and Udgaonkar, J. B. (2008) *J. Mol. Biol.* **382,** 1228–1241
68. Horcas, I., Fernández, R., Gómez-Rodríguez, J. M., Colchero, J., Gómez-Herrero, J., and Baro, A. M. (2007) *Rev. Sci. Instrum.* **78,** 013705
69. Hoshino, M., Katou, H., Hagihara, Y., Hasegawa, K., Naiki, H., and Goto, Y. (2002) *Nat. Struct. Biol.* **9,** 332–336
70. Petkova, A. T., Leapman, R. D., Guo, Z., Yau, W. M., Mattson, M. P., and Tycko, R. (2005) *Science* **307,** 262–265
71. Goux, W. J., Kopplin, L., Nguyen, A. D., Leak, K., Rutkofsky, M., Shanmuganandam, V. D., Sharma, D., Inouye, H., and Kirschner, D. A. (2004) *J. Biol. Chem.* **279,** 26868–26875
72. Naiki, H., Higuchi, K., Hosokawa, M., and Takeda, T. (1989) *Anal. Biochem.* **177,** 244–249
73. LeVine, H., 3rd (1993) *Protein Sci.* **2,** 404–410
74. Biancalana, M., Makabe, K., Koide, A., and Koide, S. (2009) *J. Mol. Biol.* **385,** 1052–1063
75. Biancalana, M., and Koide, S. (2010) *Biochim. Biophys. Acta* **1804,** 1405–1412
76. Wolfe, L. S., Calabrese, M. F., Nath, A., Blaho, D. V., Miranker, A. D., and Xiong, Y. (2010) *Proc. Natl. Acad. Sci. U.S.A.* **107,** 16863–16868
77. Pollanen, M. S., Markiewicz, P., Bergeron, C., and Goh, M. C. (1994) *Am. J. Pathol.* **144,** 869–873
78. Crowther, R. A. (1991) *Proc. Natl. Acad. Sci. U.S.A.* **88,** 2288–2292
79. Wegmann, S., Jung, Y. J., Chinnathambi, S., Mandelkow, E. M., Mandelkow, E., and Muller, D. J. (2010) *J. Biol. Chem.* **285,** 27302–27313
80. Baskakov, I. V., Legname, G., Baldwin, M. A., Prusiner, S. B., and Cohen, F. E. (2002) *J. Biol. Chem.* **277,** 21140–21148
81. Collins, S. R., Douglass, A., Vale, R. D., and Weissman, J. S. (2004) *PLoS Biol.* **2,** e321
82. Goldsbury, C., Frey, P., Olivieri, V., Aebi, U., and Müller, S. A. (2005) *J. Mol. Biol.* **352,** 282–298
83. Fersht, A. (1999) *Structure and Mechanism in Protein Science: A Guide to Enzyme Catalysis and Protein Folding*, pp. 191–215, W. H. Freeman and Co., New York
84. Frieden, C. (2007) *Protein Sci.* **16,** 2334–2344
85. Frieden, C., and Goddette, D. W. (1983) *Biochemistry* **22,** 5836–5843
86. Barshop, B. A., Wrenn, R. F., and Frieden, C. (1983) *Anal. Biochem.* **130,**

134–145
87. Chirita, C. N., and Kuret, J. (2004) *Biochemistry* **43,** 1704–1714
88. Chang, E., Kim, S., Schafer, K. N., and Kuret, J. (2011) *Biochim. Biophys. Acta* **1814,** 388–395
89. Yin, H., and Kuret, J. (2006) *FEBS Lett.* **580,** 211–215
90. Oosawa, F., and Kasai, M. (1962) *J. Mol. Biol.* **4,** 10–21
91. Kumar, S., and Udgaonkar, J. B. (2010) *Curr. Sci. India* **98,** 639–656
92. Bishop, M. F., and Ferrone, F. A. (1984) *Biophys. J.* **46,** 631–644
93. Ferrone, F. (1999) *Methods Enzymol.* **309,** 256–274
94. Rentzeperis, D., Jonsson, T., and Sauer, R. T. (1999) *Nat. Struct. Biol.* **6,** 569–573
95. Wyman, J., and Gill, S. J. (1990) *Binding and Linkage: Functional Chemistry of Biological Macromolecules*, University Science Books, Mill Valley, CA
96. Spillantini, M. G., Tolnay, M., Love, S., and Goedert, M. (1999) *Acta Neuropathol.* **97,** 585–594
97. Goedert, M., and Hasegawa, M. (1999) *Am. J. Pathol.* **154,** 1–6
98. Gosal, W. S., Morten, I. J., Hewitt, E. W., Smith, D. A., Thomson, N. H., and Radford, S. E. (2005) *J. Mol. Biol.* **351,** 850–864
99. Harper, J. D., Wong, S. S., Lieber, C. M., and Lansbury, P. T. (1997) *Chem. Biol.* **4,** 119–125
100. Nichols, M. R., Moss, M. A., Reed, D. K., Lin, W. L., Mukhopadhyay, R., Hoh, J. H., and Rosenberry, T. L. (2002) *Biochemistry* **41,** 6115–6127
101. Kumar, S., and Udgaonkar, J. B. (2009) *Biochemistry* **48,** 6441–6449
102. Santacruz, K., Lewis, J., Spires, T., Paulson, J., Kotilinek, L., Ingelsson, M., Guimaraes, A., DeTure, M., Ramsden, M., McGowan, E., Forster, C., Yue, M., Orne, J., Janus, C., Mariash, A., Kuskowski, M., Hyman, B., Hutton, M., and Ashe, K. H. (2005) *Science* **309,** 476–481
103. Yoshiyama, Y., Higuchi, M., Zhang, B., Huang, S. M., Iwata, N., Saido, T. C., Maeda, J., Suhara, T., Trojanowski, J. Q., and Lee, V. M. (2007) *Neuron* **53,** 337–351
104. Andorfer, C., Acker, C. M., Kress, Y., Hof, P. R., Duff, K., and Davies, P. (2005) *J. Neurosci.* **25,** 5446–5454
105. Lasagna-Reeves, C. A., Castillo-Carranza, D. L., Sengupta, U., Clos, A. L., Jackson, G. R., and Kayed, R. (2011) *Mol. Neurodegener.* **6,** 39
106. Taniguchi, S., Suzuki, N., Masuda, M., Hisanaga, S., Iwatsubo, T., Goedert, M., and Hasegawa, M. (2005) *J. Biol. Chem.* **280,** 7614–7623
107. Pickhardt, M., Larbig, G., Khlistunova, I., Coksezen, A., Meyer, B., Mandelkow, E. M., Schmidt, B., and Mandelkow, E. (2007) *Biochemistry* **46,** 10016–10023

SUPPLEMENTARY INFORMATION FOR

Understanding the kinetic roles of the inducer heparin and of rod-like protofibrils during amyloid fibril formation by tau

Gayathri Ramachandran and Jayant B. Udgaonkar*

From National Centre for Biological Sciences, Tata Institute of Fundamental Research, Bangalore 560065, India

Running head: Heparin-induced aggregation of tau follows a NDP mechanism

*Address correspondence to: Professor Jayant B. Udgaonkar, National Centre for Biological Sciences, Tata Institute of Fundamental Research, Bangalore 560065, India, Telephone: 91-80-23666150, Fax: 91-80-23636662, Email: jayant@ncbs.res.in

SUPPLEMENTARY METHODS

Protein purification- Briefly, *E.coli* BL21 (DE3) Star cells (Stratagene) transformed with pETtau4RPH were grown overnight at 37 °C in LB containing 100 µg/mL ampicillin and then sub-cultured into Terrific broth containing 100 µg/mL ampicillin. The cells were induced with 10 µg/ml of IPTG at an OD_{600} of 1.2-1.4, harvested 3 h later, and lysed by sonication in 50 mM PIPES-NaOH buffer containing 50 mM NaCl, 1mM EDTA, 5 mM DTT, 0.1 mM PMSF, pH 6.9. The crude filtered lysate obtained following centrifugation, was then loaded onto a SP-Sepharose FF (Sigma) cation exchange column and eluted against a gradient of 0 to 250 mM NaCl. Fractions that contained tau4RD, as determined by SDS-PAGE were pooled, concentrated to around 7.5 mg/ml in a stirred ultra-filtration cell with an YM3 filter (Amicon), and loaded onto a Hiload 16/60 Superdex 75 preparative grade column (Amersham Biosciences). The tau4RD fractions were pooled, flash frozen in liquid N_2 and stored at -80°C in the elution buffer (25 mM Tris buffer, pH 7) without any further concentration steps.

Aggregation in PBS buffer- For the studies involving aggregation in PBS buffer (10 mM Na_2HPO_4, 2 mM KH_2PO_4, 137 mM NaCl, 3 mM KCl, pH 7.4), the protein stored in 25 mM Tris buffer was buffer-exchanged into PBS using a PD-10 column (Amersham Biosciences). The protein was then diluted into the aggregation buffer (PBS, 1 mM DTT, pH 7.4) to the desired concentration. After an incubation of 3 h at 37 °C, the reaction was induced by the addition of heparin at a final concentration of 37.5 µM. The final pH was 7.4 and the aggregation reaction continued to be maintained at 37 °C. It was seen that if the initial incubation in DTT was varied from 1 to 3 h, it made no difference to the process measured. AFM samples of fibrils formed in PBS were made of aliquots withdrawn at 60 h, the time corresponding to $3t_{50}$ as determined from ThT fluorescence monitored kinetics.

Atomic Force Microscopy (AFM)- A small scanner (Agilent technologies) with a maximum scan size of ~10 µm was used for acquiring most of the images; for some, a large scanner (Agilent technologies) with a maximum scan size of ~100 µm was used. Image acquisition parameters: scan speed, 1.0-1.5 lines/second; pixel intensity, minimum of 512 data points/line, for most images: 1024 data points/line. All AFM images are shown in the topography format unless otherwise specified. The determination of each height distribution involved measurements on ~100 fibrils or ~200 protofibrils. All images were flattened using the flatten filter option of WSxM (1), but no further processing was carried out. Fibril and protofibril diameters were measured along the direction perpendicular to their lengths. Fibrils formed in Tris buffer were found to have a tendency to form clumps. While measuring heights from fibril clumps, only those fibrils were included in the height analysis that could be distinguished as single fibers with no other fibrils forming a mat beneath. This sampling technique thus had an inherent bias built in for sampling individual fibrils at the edges of clumps or for sampling individual fibrils that lay scattered on the mica in some frames of view. This bias was however maintained uniformly for all the fibril images analyzed. The lengths of protofibrils were also measured using WsXM. In order to make a clear distinction between fibrils and protofibrils, fragments that were < 100 nm in length, even if they possessed heights > 5 nm were not considered to

be fibrils. It was not possible to reliably measure fibril lengths as a result of the tendency of fibrils to clump.

Fourier Transform Infrared (FTIR) Spectroscopy- FTIR measurements were carried out in the thin film attenuated total reflectance (TF-ATR) mode as previously described (2). Briefly, FTIR spectra were collected on a Thermo-Nicolet-6700 FT-IR spectrometer (Thermo Scientific) equipped with a liquid N_2-cooled MCT detector and a Smart Orbit ATR accessory. The instrument was purged with ultra-pure nitrogen for 1 h before the start of the experiment, to remove residual CO_2 and water vapor, and the purge was left on while acquiring spectra. Acquisition parameters: interferograms averaged, 1024; resolution, 4 cm^{-1}.

FTIR spectra of the fibril samples were acquired at times corresponding to five time constants (5τ) of the ThT fluorescence monitored kinetics for the Tris reactions and at the time corresponding to $3t_{50}$ of ThT fluorescence monitored kinetics for the PBS reaction. At the designated times, 0.5 ml aggregation reactions were spun down at 25,000g for 15 min to pellet the fibrils, the pellet was then re-suspended in 10 µl of the supernatant in the case of Tris reactions and 5 µl in the case of PBS reactions. 3 µl of the suspension was used to prepare a thin film by drying the sample under a gentle stream of N_2, after spreading it evenly over the diamond crystal. For each sample, a thin film of the appropriate buffer was used as a blank before sample acquisition. Control experiments were performed to confirm that the shape of the spectra remains the same irrespective of the volume of suspension dried to form a thin film.

Data Analysis of PBS reactions- For the aggregation reactions in PBS, the kinetic curves measured by ThT fluorescence were fitted to the sigmoidal equation

$$S = \frac{S_\infty}{1 + e^{-((t - t_{50})/\tau)}} \quad (1)$$

where S_∞ is the amplitude of signal change, t is the time, t_{50} is the time at which the change in signal is 50%, and τ is a characteristic time constant.

The amplitude of the change in signal determined from fitting the data to equation 1 was used to calculate the fractional change at each time point using the equation:

$$Fractional\ change = \frac{S}{S_\infty} \quad (2)$$

SUPPLEMENTARY TEXT

Aggregation in PBS buffer follows sigmoidal kinetics. Aggregation in PBS buffer, as monitored by ThT fluorescence, follows sigmoidal kinetics with a distinct lag phase (Supplementary Figure 1a). Across different protein preparations, the one feature of the kinetic process that remained inviolate in the PBS buffer is the t_{50} value, and when different experiments are normalized for their difference in amplitude by calculating the fractional change in the ThT signal, the kinetic traces of aggregation overlap well with each other (Supplementary Figure 1a, inset).

Salt modulates aggregation kinetics in Tris buffer. As expected for an aggregation reaction where the protein is basic and the inducer is a polyanion, the ionic strength of the solution modulates aggregation kinetics (Supplementary Figure 1b). This result is consistent with previous observations (3,4) that the aggregation reaction is modulated by electrostatic interactions. In Tris buffer at pH 7, the aggregation reaction is fastest in 50 mM NaCl; at 150 mM NaCl and higher NaCl concentrations, the electrostatic interactions between tau4RD and heparin are screened and hence the aggregation process is greatly slowed down. At lower concentrations of salt (< 50 mM), the aggregation reaction

accelerates with increasing salt concentration, presumably because the presence of the low concentration (< 50 mM) of salt results in some compaction of the protein, making it more conducive for aggregation. DLS distributions in the absence and presence of salt do not, however, show any apparent difference in the mean R_H (data not shown).

Fibrils formed in PBS and Tris possess distinct FTIR spectra but similar thicknesses. The thin film ATR-FTIR spectra of the final fibrillar structures formed at a time corresponding to 5 times the time constant of ThT kinetics in Tris buffer and at a time corresponding to 3 times the t_{50} of ThT kinetics in PBS show interesting differences (Supplementary Figure 2a, c). The position of the amide I band assigned to β-sheet structures is at 1626 cm^{-1} in the case of the Tris fibrils while in the case of the PBS fibrils, it is at 1632 cm^{-1}. This difference is significant and suggests that the internal structures of fibrils formed in Tris and PBS buffers may be different. In addition, the ATR-FTIR spectra of Tris fibrils displays a shoulder at 1655 cm^{-1} that is absent in the case of the PBS fibrils. This amide I band is generally assigned to α-helical and/ or random coil structures. Hence, it appears that the Tris fibrils possess a mixture of α-helical/ random coil and β-sheet structures, while the PBS fibrils are largely composed of β sheet structures.

Fibrils are formed in both Tris and PBS buffers (Supplementary Figure 2b, d) but fewer fibrils are formed in the case of PBS, a pattern that seems consistent with the difference in ThT fluorescence amplitudes seen for the two buffers. The fibrils formed in Tris buffer consist of a mixture of single fibrils and laterally-associated fibrils; clumps of fibrils (Supplementary Figure 2b, inset) are a characteristic feature of aggregation in Tris buffer. In contrast, the fibrils formed in PBS are not as densely clumped because they are fewer in number (Supplementary Figure 2d, inset). Further, while the average height of fibrils formed in Tris buffer is ~10 nm that of fibrils formed in PBS varies across protein preparations, from 6-10 nm (data not shown). This variation appears, however, to be correlated with the variation in ThT fluorescence amplitude across different protein preparations.

Fibrils formed over a range of heparin concentrations are not significantly different in their thicknesses. AFM images of fibrils formed in Tris buffer in the presence of 8.3, 37.5 and 75 μM heparin, which represent the three points of the bell-shaped curve (Figure 5b), indicate that the fibrils are largely similar in their heights, irrespective of the heparin concentration at which they are formed (Supplementary Figure 3). Fibrils formed at all heparin concentrations seem to possess a similar tendency to clump as well (insets of Supplementary Figure 3a, b, c).

Fibrils formed at different protein concentrations are not significantly different in their thicknesses. AFM images of fibrils formed at two different protein concentrations (10 and 90 μM) when aggregated at a fixed concentration of heparin (37.5 μM), indicate that the heights of the fibrils are not significantly altered across the two conditions (Supplementary Figure 4). The fibrils form clumps in both conditions as well (insets of Supplementary Figure 4a, b).

Fibrils formed at different molar ratios of protein: heparin possess similar internal structures. FTIR spectra of fibrils formed at three different molar ratios of protein to heparin (0.27, 1.33, 6.0), that represent the two extremes and the peak of the bell-shaped curve (Figure 7), appear to be very similar (Supplementary Figure 5a, b, c). Irrespective of the stoichiometry of protein to polyanion, all three spectra show the presence of a β-sheet contribution at 1626 cm^{-1} and an α-helical/ random coil contribution at 1655 cm^{-1}.

Kinetic simulations support the proposed mechanism of aggregation. A simple kinetic simulation was carried out to test the basic features of the proposed mechanism (Supplementary Figure 6), namely the dependences of the aggregation kinetics (apparent rate constants as well as relative amplitudes) on protein and heparin concentrations. The scheme used describes the formation of a hexamer P_6H in the presence of heparin, and hence, shows the minimum number of growth steps that need to be included to account for the data over the ranges of protein and heparin concentration wherein aggregation kinetics were measured. The off-pathway intermediate is a tight-binding P*H

complex. The rate-limiting step of this reaction is the formation of the aggregation competent dimer PHP; further elongation to form P_6H would occur at a much faster rate and by the addition of monomers. As can be seen, the simulation is able to correctly predict all the important features of the observed kinetic data (Supplementary Figure 7). Kinetic simulations to a model incorporating the other kind of off-pathway intermediate that is likely to be formed, an aggregation-incompetent protein dimer, PP (Scheme 3), gave dependences of the kinetics on protein and heparin concentration, similar in pattern to the simulations shown, indicating that either of the mechanisms can equally well explain the observed data.

SUPPLEMENTARY REFERENCES

1. Horcas, I., Fernandez, R., Gomez-Rodriguez, J. M., Colchero, J., Gomez-Herrero, J., and Baro, A. M. (2007) *Rev Sci Instrum* **78**, 013705

2. Seshadri, S., Khurana, R., and Fink, A. L. (1999) *Methods Enzymol* **309**, 559-576

3. Jeganathan, S., von Bergen, M., Mandelkow, E. M., and Mandelkow, E. (2008) *Biochemistry* **47**, 10526-10539

4. Andronesi, O. C., von Bergen, M., Biernat, J., Seidel, K., Griesinger, C., Mandelkow, E., and Baldus, M. (2008) *J Am Chem Soc* **130**, 5922-5928

SUPPLEMENTARY FIGURE LEGENDS

Figure 1: (a) ThT-fluorescence monitored kinetics of fibril formation by 50 µM tau4RD in the presence of 37.5 µM heparin in PBS buffer containing 1 mM DTT, pH 7.4 at 37 °C. The inset shows a plot of fractional change in ThT signal averaged across two different protein preparations. (b) Dependence of ThT fluorescence monitored kinetics in 25 mM Tris buffer, 1 mM DTT, pH 7 on NaCl concentration. The continuous line through the data points was drawn by inspection.

Figure 2: FTIR spectra and AFM images of fibrils formed in Tris, pH 7 and in PBS, pH 7.4. (a) FTIR spectra of fibrils formed in Tris, pH 7 acquired at a time corresponding to 5 time constants of ThT fluorescence- monitored kinetics. The lines drawn through the spectra at 1626 cm^{-1} and 1655 cm^{-1} represent the positions expected for β-sheet rich structures and α-helical/ random coil structures respectively. (b) AFM image of fibrils formed in Tris buffer, at a time corresponding to 5 time constants of ThT fluorescence-monitored kinetics. The inset shows an image of a clump of fibrils formed at the same time point, but imaged from a separate sample preparation. (c) FTIR spectra of fibrils formed in PBS, pH 7.4 acquired at a time corresponding to 3 times the t_{50} of ThT fluorescence-monitored kinetics. The line drawn through the spectra at 1632 cm^{-1} represents the position expected for β-sheet rich structures. (d) AFM image of a fibril formed at a time corresponding to 3 times the t_{50} of ThT fluorescence-monitored kinetics in PBS. The inset depicts a set of fibrils from a different region of the mica, formed at the same time point and imaged from the same sample preparation. The scale bar in both images and insets of (b) and (d) corresponds to 600 nm. The Z scale for images and insets in both (b) and (d) has been set to 50 nm to facilitate a visual comparison of the thickness of the fibrils. If required, the Z scale has been offset to ensure that the mica background is of a similar color across images. The color scale in the images corresponds to the main image.

Figure 3: AFM images of fibrils formed at three different heparin concentrations that span the concentration range studied (a), (b) and (c) AFM images of fibrils formed at 8.3 µM, 37.5 µM and 75 µM heparin, respectively. The images were acquired at times corresponding to 5 time constants of ThT fluorescence-monitored kinetics. The insets in (a), (b) and (c) show clumps of fibrils formed in the respective conditions. The scale bar in all images and insets corresponds to 600 nm. The Z scale

for all images corresponds to 50 nm and that for all insets, to 75 nm to facilitate visual comparison of the thicknesses of the fibrils. The color scale in the images corresponds to the main image and if required, the Z scale has been offset to ensure that the mica background is of a similar color across images. (d), (e) and (f) show the height distributions of fibrils formed in conditions described in (a), (b) and (c) respectively. The mean heights of the fibrils, determined from the Gaussian fits, are 12.8 ± 1.8 nm, 9.1 ± 2.9 nm and 8.7 ± 2.3 nm respectively. All height measurements were made from images similar to the one shown as the main image; none of the height measurements were made from images shown as insets. The solid lines represent fits to a Gaussian equation. These mean heights, given the inherent error associated with the measurement technique, are not considered to be significantly different.

Figure 4: AFM images of fibrils formed at different protein concentrations (a) and (b) AFM image of fibrils formed by 10 and 90 μM tau4RD in the presence of 37.5 μM heparin at a time corresponding to 5 time constants of ThT fluorescence-monitored kinetics. The inset shows clumps formed in the respective conditions. The scale bar in both the images and insets correspond to 600 nm. The Z scale of the images corresponds to 50 nm and that of the insets, to 75 nm. The color scale corresponds to the main image and if required, the Z scale has been offset such that the color of the mica background appears similar across the images. (c) and (d) show the distribution of heights of fibrils corresponding to (a) and (b) respectively. The mean heights of the distributions, calculated from the fits, are 9.8 ± 2.5 nm and 7.8 ± 2.2 nm, respectively. All height measurements were made from images similar to the ones shown as the main image. None of the height measurements were made from the inset images. The solid line represents a fit to a Gaussian equation. These mean heights, given the inherent error associated with the measurement technique, are not considered to be significantly different.

Figure 5: FTIR spectra of fibrils formed at different molar ratios of protein to heparin, at 50 μM tau4RD concentration (a) FTIR spectra of fibrils formed by 50 μM tau4RD, 187.5 μM heparin (molar ratio of 0.27), at a time corresponding to 5 time constants of ThT fluorescence-monitored kinetics determined for 10 μM tau4RD, 37.5 μM heparin (b) FTIR spectra of fibrils formed by 50 μM tau4RD, 37.5 μM heparin (molar ratio of 1.33) at a time corresponding to 5 time constants of ThT fluorescence-monitored kinetics (c) FTIR spectra of fibrils formed by 50 μM tau4RD, 8.3 μM heparin (molar ratio of 6.0) at a time corresponding to 5 time constants of ThT fluorescence-monitored kinetics. The lines drawn through the spectra at 1626 cm^{-1} and 1655 cm^{-1} represent the positions expected for β-sheet rich structures and α-helical/ random coil structures, respectively.

Figure 6: Mechanism used for kinetic simulation. The mechanism is a minimalistic model, showing aggregation to proceed to the extent of a hexamer of protein (P) in the presence of heparin (H). The off-pathway intermediate whose formation has been simulated is a tight-binding P^*H complex. The values of the rate constants used in the simulation are as shown in the table.

Figure 7: Kinetic simulations supporting the mechanism of aggregation of tau4RD in the presence of heparin. In panels a-e, experimental data from Figures 5-7 (white symbols) have been shown along with the data from kinetic simulations (black symbols). (a) The apparent rate constants of ThT monitored kinetics plotted against heparin concentration. The apparent rate constants of both the experimental data and the simulation data have been normalized to their respective rate constants at 16.6 μM heparin. (b) The apparent rate constants of ThT monitored kinetics plotted against protein concentration. The apparent rate constants of both the experimental and the simulation data have been normalized to their respective rate constants at 60 μM protein. (c) The apparent rate constants of ThT monitored kinetics plotted against the molar ratio of protein to heparin. The apparent rate constants of both the experimental and the simulation data have been normalized to their respective rate constants at 60 μM protein. (d) The amplitudes of change in ThT fluorescence plotted against heparin concentration. The ThT amplitudes for both the experimental and the simulation data have been normalized to their respective amplitudes at 16.6 μM heparin. (e) The amplitudes of change in ThT

fluorescence plotted against protein concentration. The ThT amplitudes of both experimental and the simulation data have been normalized to their respective amplitudes at 60 μM protein.

Supplementary Figure 1

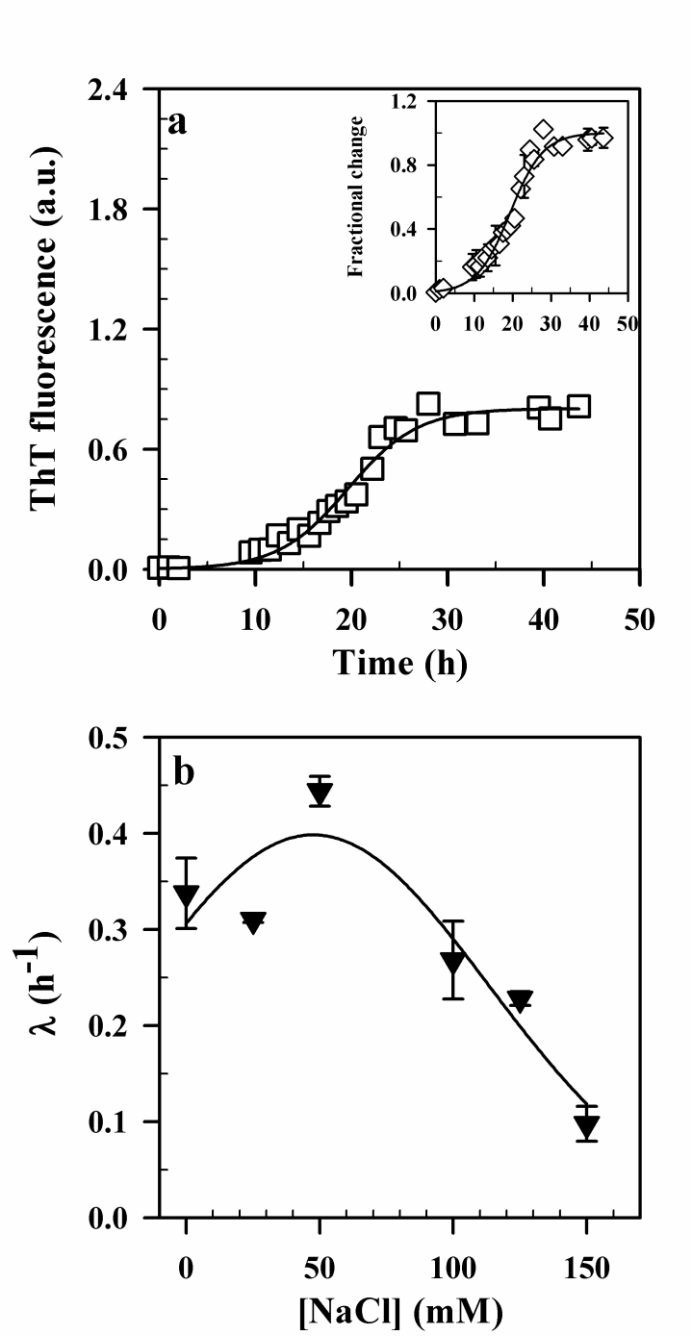

Supplementary Figure 2

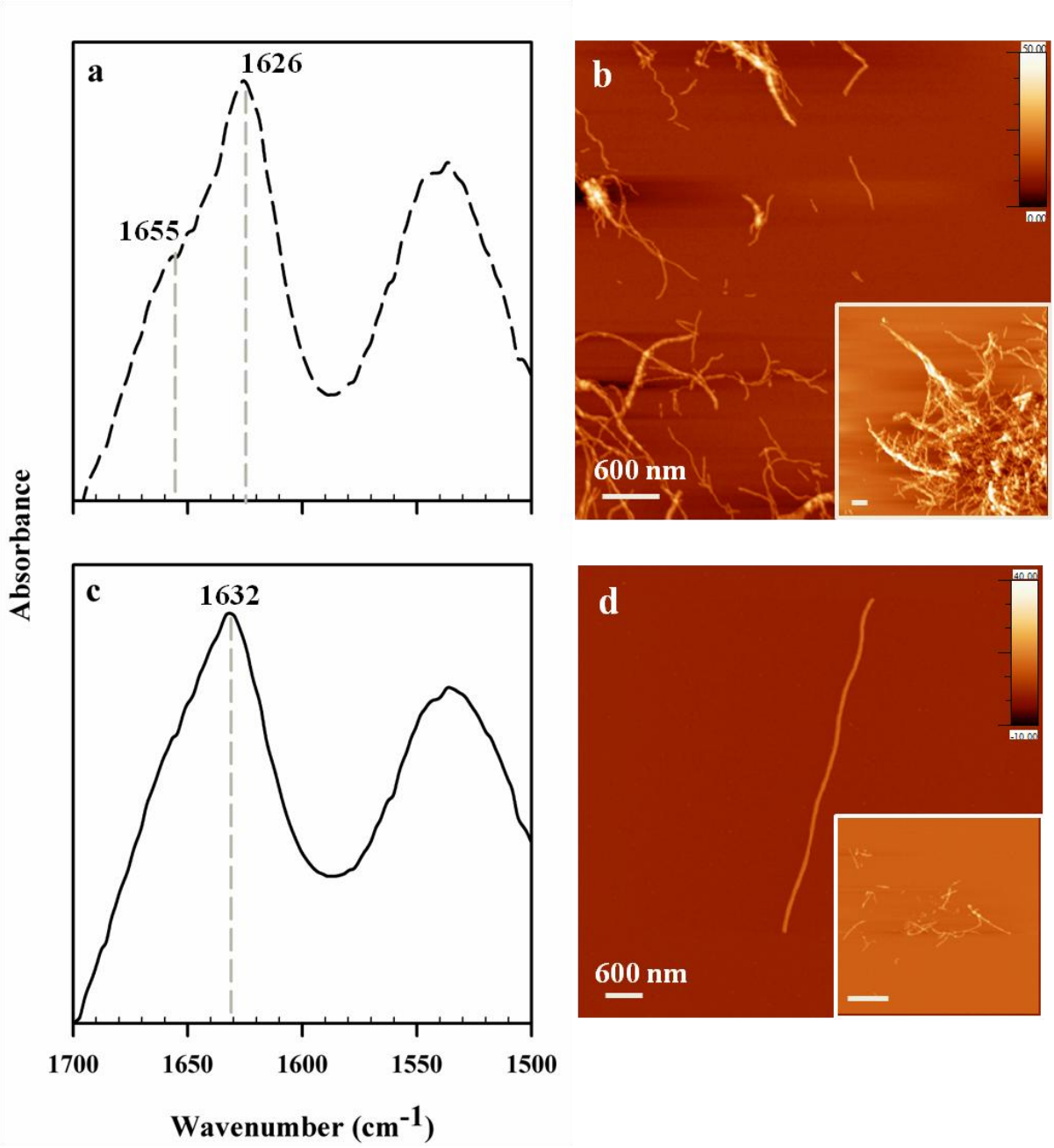

Supplementary Figure 3

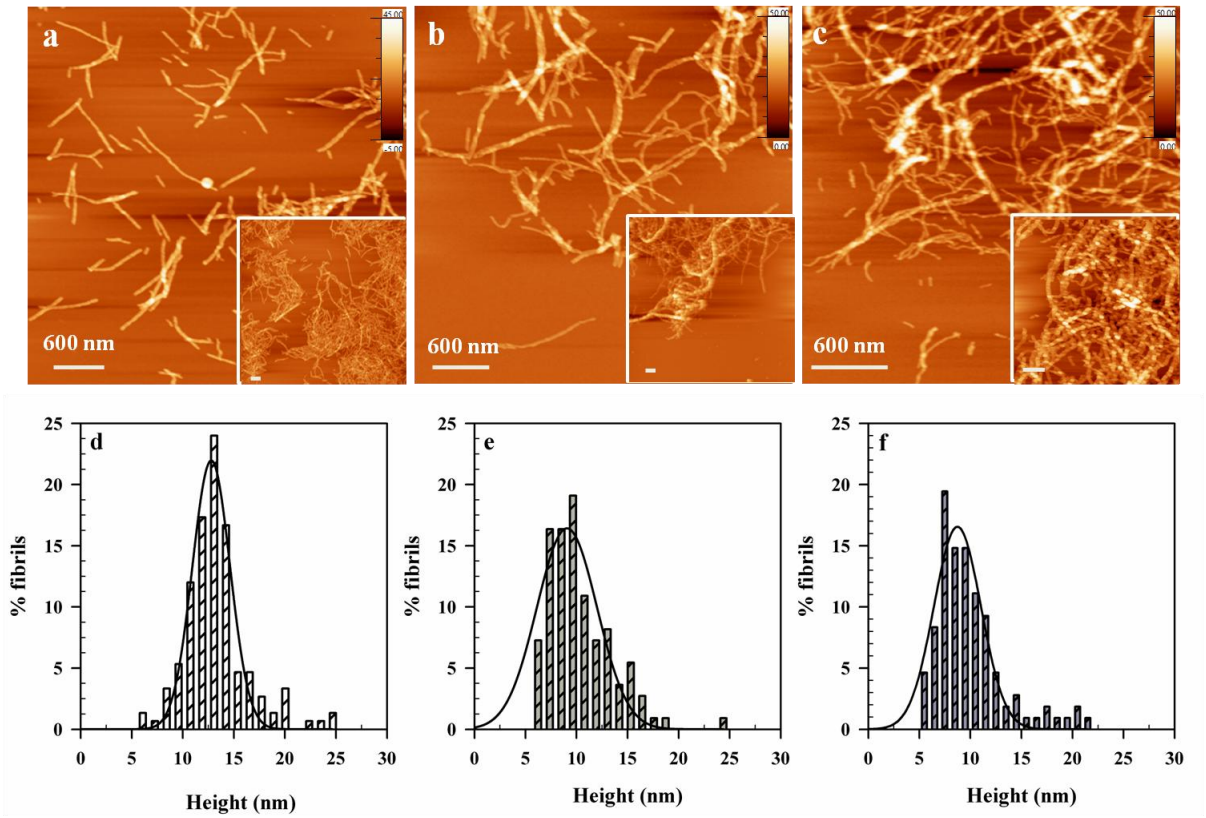

Supplementary Figure 4

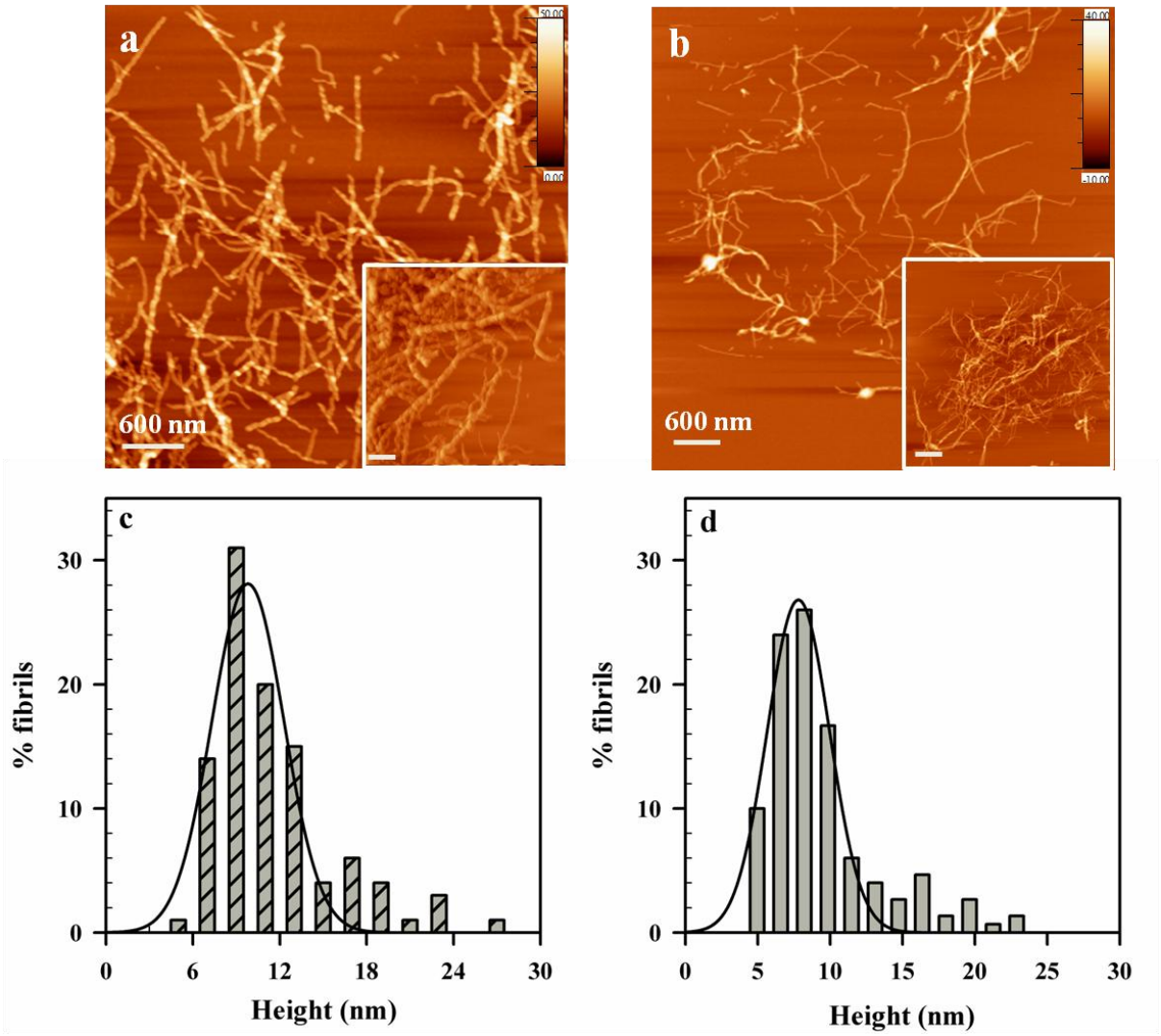

Supplementary Figure 5

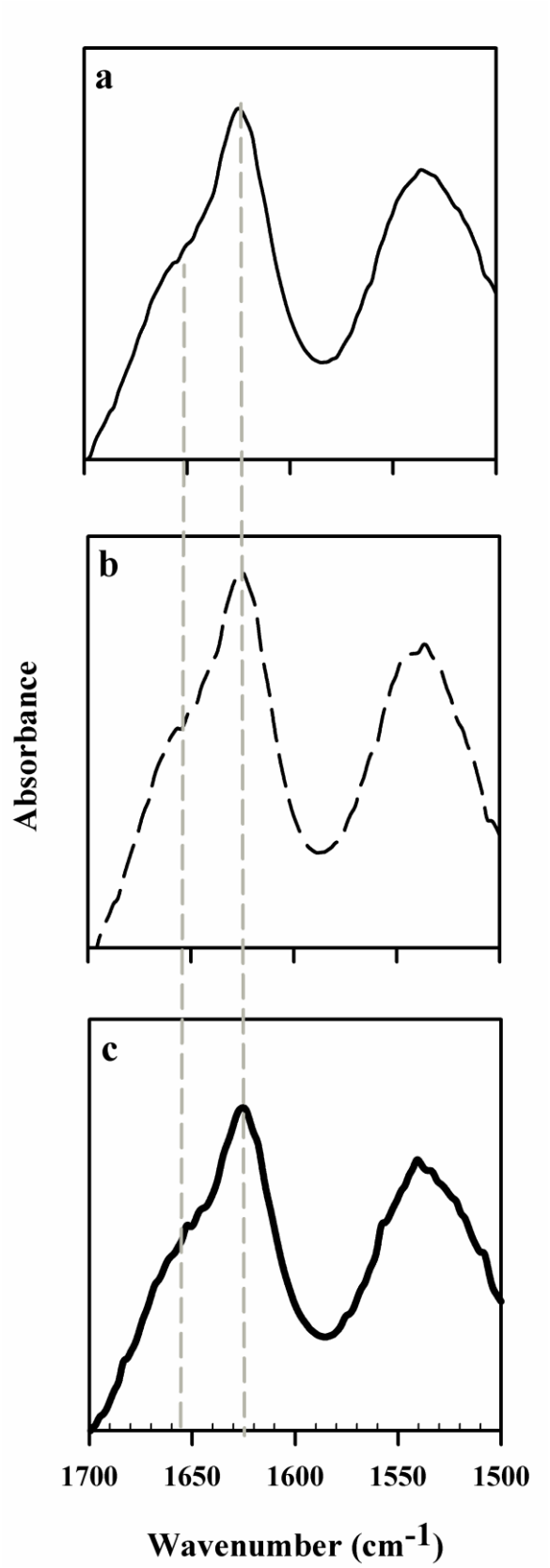

Supplementary Figure 6

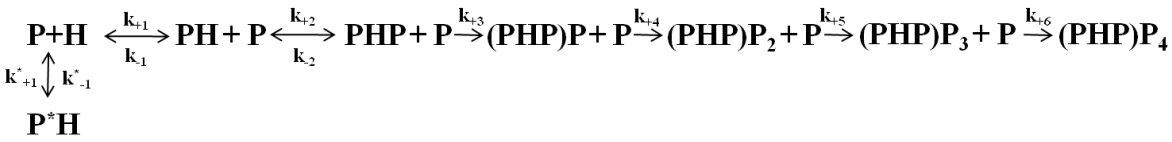

Rate constant	Value
k_{+1}	10 μM^{-1} h^{-1}
k_{-1}	5 h^{-1}
k^{*}_{+1}	500 μM^{-1} h^{-1}
k^{*}_{-1}	5 h^{-1}
k_{+2}	250 μM^{-1} h^{-1}
$k_{+3}=k_{+4}=k_{+5}=k_{+6}$	2500 μM^{-1} h^{-1}
$k_{-2}=k_{-3}=k_{-4}=k_{-5}=k_{-6}$	0.005 h^{-1}

Supplementary Figure 7